[American Journal of Science, Vol. 314, January, 2014, P. 154–186, DOI 10.2475/01.2014.05]

EARLY PALEOZOIC DEPOSITIONAL ENVIRONMENT AND INTRAPLATE TECTONO-MAGMATISM IN THE CATHAYSIA BLOCK (SOUTH CHINA): EVIDENCE FROM STRATIGRAPHIC, STRUCTURAL, GEOCHEMICAL AND GEOCHRONOLOGICAL INVESTIGATIONS

L. S. SHU*,†, B. M. JAHN**, J. CHARVET***, M. SANTOSH§, B. WANG*, X. S. XU*, and S. Y. JIANG*

ABSTRACT. The early Paleozoic geological evolution of the South China Craton composed of the Yangtze and Cathaysia Blocks has been the focus of long debate. The Cathaysia block has been central to the controversy regarding convergent margin versus intraplate environment in the early Paleozoic. In order to address the early Paleozoic evolution of Cathaysia, we undertook a systematic study of the stratigraphic sequences, deformational features and geochronology of magmatic event. Our results show that (1) during the early Paleozoic, the Jiangnan domain of the SE Yangtze block was characterized by a carbonate platform and the Cathaysia block by a graptolite-facies clastic rock assemblage, (2) in the Cathaysia block, a littoral-neritic depositional environment prevailed in Cambrian whereas a neritic-bathyal setting dominated during the early-middle Ordovician, and (3) the Late Ordovician depositional sequence in Cathaysia witnessed a period of transition from neritic-bathyal to littoral-land environment, marking the initial uplift process. Paleo-current measurements on the crossbeds revealed northwestward and westward transport directions, suggesting a source area to the east-southeast. All samples collected from the Cambrian-Ordovician strata show similar chemical characteristics; they have negative $\varepsilon_{Nd}(t)$ values (−9.7 to −13.7) and two-stage εNd(t) model ages at *ca*.2.04 to 2.36 Ga. This suggests that the early Paleozoic rocks were derived from the eroded Paleoproterozoic basement, and little or no mantle component was identified. During the Silurian, the Cathaysia block underwent strong folding, thrusting, weak metamorphism and large-scale anatexis accompanied by granitoid emplacement, building the South China Fold Belt. The maximum shortening is estimated at 67 percent. A kinematic analysis of the ductile sheared rocks revealed a fan-shape thrust pattern, with top-to-the southeast in the southeastern and top-to-the northwest in the northwestern Cathaysia block. Zircon U-Pb dating of four granitic plutons yielded $^{206}Pb/^{238}U$ ages of 435 ± 4 Ma, 424 ± 5 Ma, 428 ± 3 Ma and 427 ± 2 Ma. All the zircon εHf(t) values are negative (−6 to −9) and show a peak of two-stage Hf model ages around 1.9 Ga, indicating that the Silurian granitic magma was derived from the recycling of Paleoproterozoic basement. Major features of the early Paleozoic South China Fold Belt include the lack of early Paleozoic ophiolites and volcanic rocks, the absence of coeval HP-type blueschists, and the absence of mantle-derived juvenile magmatic rocks. Consequently, a subduction-collision-type orogeny is excluded. The magmatism most probably took place in an intraplate tectonic setting with little or no input of mantle components. We therefore conclude that the South China Fold Belt was an intraplate orogen, and is possibly related to the global early Paleozoic continental assembly.

Key words: Depositional sequence, ductile deformation, intraplate magmatism, geodynamic evolution, early Paleozoic, South China Fold Belt, Cathaysia block

* State Key Laboratory for Mineral Deposits Research, Nanjing University, Nanjing 210093, P. R. China
** Department of Geosciences, National Taiwan University, P.O. Box 13-318 Taipei, 106 Taiwan
*** Institut des Sciences de la Terre d'Orléans, UMR 7323—CNRS/Université d'Orléans, 1A, rue de la Férollerie, 45071 Orléans cedex 2, France
§ School of Earth Sciences and Resources, China University of Geosciences Beijing, No. 29, Xueyuan Road, Haidian District, Beijing 100083, P. R. China
† Corresponding author: E-mail: lsshu@nju.edu.cn; Fax: 86-25-83686016

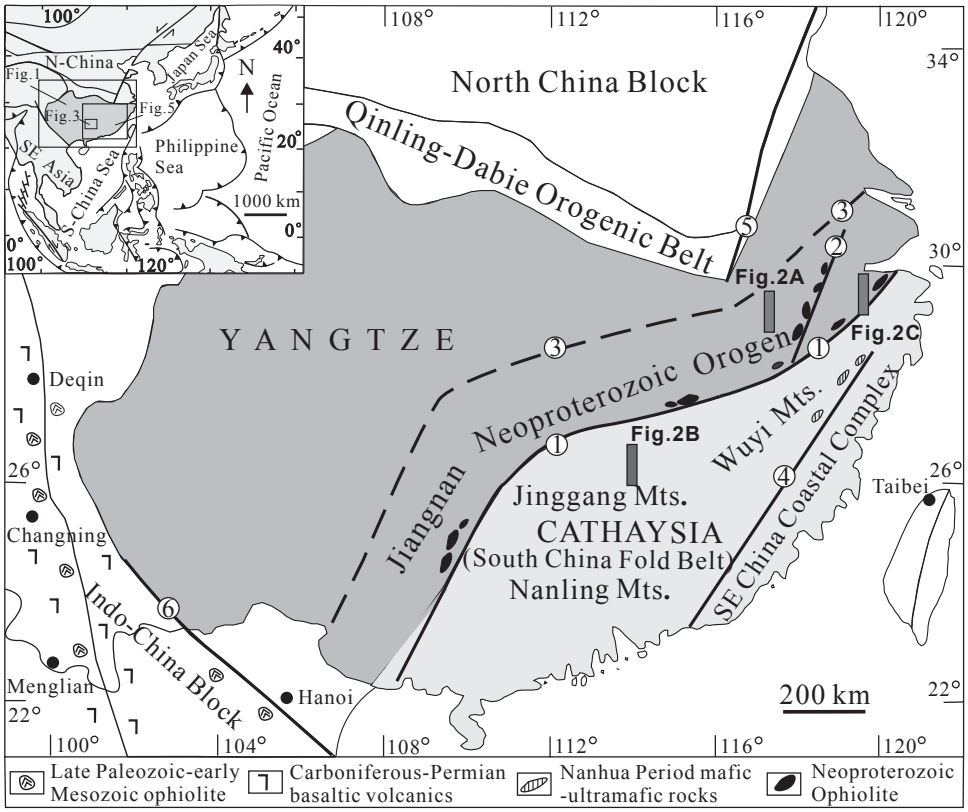

Fig. 1. Tectonic framework of the South China Craton. ①, Shaoxing-Jiangshan-Pingxiang fault zone; ②, Dongxiang-Dexing fault zone; ③, The buried fault zone as a northern boundary of Jiangnan belt; ④, Zhenghe-Dapu fault zone; ⑤, Tan-Lu fault zone; ⑥, Songma fault zone.

INTRODUCTION

The South China Craton consists of the Yangtze and Cathaysia blocks and has been the focus of many recent studies in relation to global tectonics, especially the Rodinia supercontinent history (for example, Guo and others, 1989; Gilder and others, 1991; Xiao and He, 2005; X. H. Li and others, 2009; Z. X. Li and others, 2010; W. X. Li and others, 2010; D. Y. Liang and others, 2011; Yao and others, 2011; Wang and others, 2013). The NE-trending South China Fold Belt (Ren and others, 1990, 1998; H. Z. Wang and Mo, 1995) is an early Paleozoic orogen with a regional-scale angular unconformity between Devonian conglomerates and pre-Devonian metamorphic units. This orogen occupies almost the whole Cathaysia block covering an area of more than 300,000 km^2 and evolved from the Proterozoic basement of Cathaysia (Faure and others, 2009; Charvet and others, 2010; Shu and others, 2011a). The basement of Cathaysia witnessed extensive reworking through folding, thrusting and magmatism in the early Paleozoic, with large scale anatexis and emplacement of granitoids in Silurian. This event is well recorded in the Wuyi, Jinggang and Nanling areas (fig. 1) (Shu, 2006; Shu and others, 2008a, 2008b; Faure and others, 2009; Charvet and others, 2010; Y. Zhang and others, 2011; X. B. Xu and others, 2011).

The South China Fold Belt, with a width of 200 to 600 km, was initially termed "Cathaysia" by Grabau. It includes the South China Basin, Taiwan, the Yellow Sea and

Japan (Grabau, 1924) and was considered to be an "old land" of Precambrian age. In the early 1970's, Jahn suggested that the Cathaysia was composed mainly of the early Paleozoic Guangxi-Hunan-Jiangxi and the Guangdong-Fujian fold belts that underwent a strong Mesozoic thermal event, forming large-scale volcanic rocks associated with intrusive granites along the coastal region of southeast China (Jahn, 1974). Earlier models correlated this younger event with the northwestward subduction of the Pacific plate (Jahn, 1974, 2010; Jahn and others, 1976).

The tectonic history of the South China Fold Belt has been extensively debated in the last two decades, and several tectonic models have been proposed such as an early Paleozoic fold belt (Ren and others, 1990, 1998), an early Paleozoic active continental margin or trench-arc system (Guo and others, 1989; H. Z. Wang and Mo, 1995), an early Mesozoic collision orogen (Hsu and others, 1988), a multiphase collision orogen (B. Xu and others, 1992) and an early Paleozoic collision orogen (J. L. Li, 1993). Recent studies consider the South China Fold Belt as an intra-continental orogen (Shu and others, 2008a; Faure and others, 2009; Z. X. Li and others, 2010; Charvet and others, 2010; X. B. Xu and others, 2011).

Most debates on the tectonic setting have focused on two major aspects: (1) the depositional environment in South China during the early Paleozoic, and (2) the geodynamic processes responsible for early Paleozoic deformation, metamorphism and magmatism. In this paper, we document the results from our field investigations on the depositional sequences and sedimentary structures. We also provide new geochemical data for the sedimentary rocks and zircon U-Pb ages from the granitoid rocks in the Nanling and Wuyi areas. These data are then used to constrain the depositional environment, tectono-magmatic event and crustal evolution of the South China Fold Belt during the early Paleozoic.

TECTONIC SETTING

Pre-Devonian Geological Background

The South China Fold Belt is separated from the Neoproterozoic Jiangnan orogen of the Yangtze Block to the northwest (for example, Yao and others, 2011; Xu and others, 2013; Zhang and Zheng, 2013), and covered by the SE China Coastal Complex to the southeast. Our study area is located in the eastern part of the South China Fold Belt, covering the Jinggang, Nanling and Wuyi Mountains (hereafter referred to as Jinggang, Nanling and Wuyi) (fig. 1). The early Paleozoic strata are mainly distributed in Jinggang and Nanling whereas Proterozoic basement rocks are widely exposed in Wuyi (JXBGMR, 1984; FJBGMR, 1985; HNBGMR, 1987; GDBGMR, 1988; ZJBGMR, 1989). Two pre-Devonian litho-tectonic units have been recognized in the South China Fold Belt (Faure and others, 2009; Shu and others, 2011a): (1) a slate unit, composed of the Sinian (the latest Neoproterozoic) to Ordovician marine facies sandy-muddy rocks, which underwent low grade metamorphism and was intruded by the Silurian granitoids, (2) a basement unit, comprising Neoproterozoic mica schist, amphibolite, paragneiss and orthogneiss, and locally with Paleoproterozoic amphibolites, gneisses and gneissic granites, which mainly occur in the northern Wuyi (X. H. Li, 1998; Yu and others, 2009).

The northwestern boundary of the South China Fold Belt was considered as an early Neoproterozoic suture zone (Guo and others, 1989) between the Yangtze and Cathaysia blocks. The suture zone is customarily called the Shaoxing-Jiangshan-Pingxiang zone (fig. 1) and is composed of several Neoproterozoic lithotectonic associations including turbidites, ophiolitic blocks with isotopic ages of 970 to 890 Ma (J. F. Chen and others, 1991; X. H. Li and others, 1994; Shu and others, 1995, 2006, 2011a; X. L. Wang and others, 2007), arc-type granites and rhyolites dated at 910 to 880 Ma (W. X. Li and others, 2008), HP/LT blueschists with the metamorphic age of 866 ±

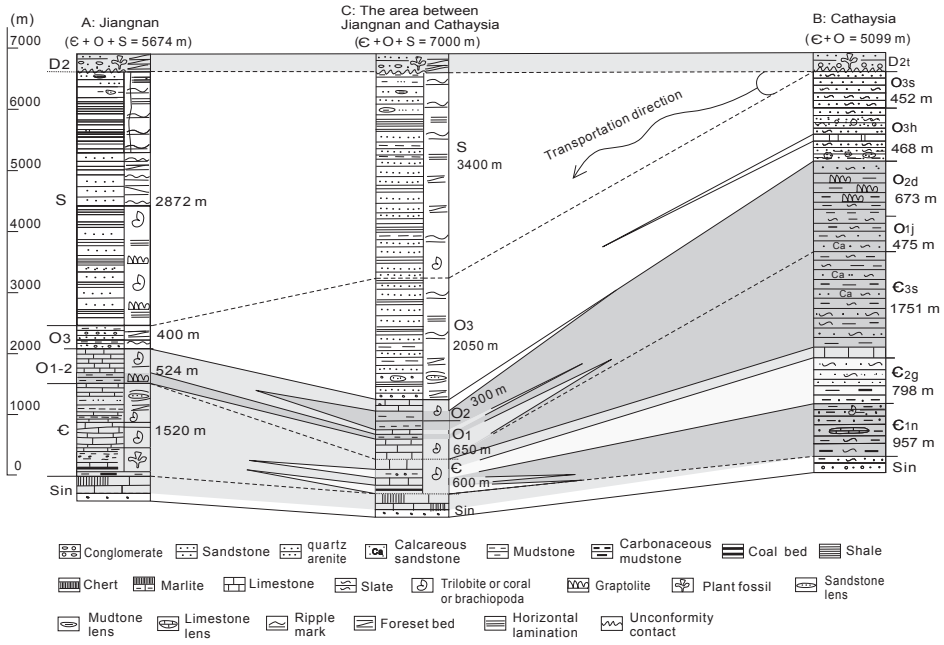

Fig. 2. Three early Paleozoic depositional sequences from the Jiangnan, the Cathaysia and the intervening zone.

14 Ma (Shu and others, 1994; Shu and Charvet, 1996) and numerous post-collisional granites with U-Pb ages from 830 to 790 Ma (X. L. Wang and others, 2006; Shu, 2006; X. H. Li and others, 2009).

The late Neoproterozoic was proposed by Gilder and others (1991) to be a significant period of rifting. This interpretation was later supported by the finding of several mafic-ultramafic and granitic bodies dated at 850 to 800 Ma (Z. X. Li and others, 2003; Shu, 2006; X. L. Wang and others, 2006; W. X. Li and others, 2005; Shu and others, 2011a). The rifting was related to the breakup of the entire South China Block as a response to the breakup of Rodinia supercontinent, and triggered the eruption of bimodal volcanic rocks at 810 to 790 Ma (J. Wang and Li, 2003; W. X. Li and others, 2005; Shu and others, 2008b).

After the late Neoproterozoic breakup, three types of depositional sequences formed in the Jiangnan, Cathaysia and intervening zones. The Jiangnan domain is characterized by a carbonate platform, and is distinct from the Cathaysia domain where a deep-water, graptolite-bearing sandy-muddy siliciclastic succession was accumulated. The intervening zones between Jiangnan and Cathaysia show a transitional depositional sequence (fig. 2).

Polyphase Magmatic Events

Subsequent to the early Paleozoic evolution, three major tectono-magmatic events took place in South China. The first led to the folding and deformation of all pre-Devonian strata, forming an anticlinorium with an E-W-trending axis that was followed by strong thrusting. This was an important early Paleozoic orogenic event, which was accompanied by greenschist facies metamorphism and voluminous S-type

granitic intrusions. Zircon U-Pb and mica Ar-Ar dating of granitoids, gneissic granites and mica schists yielded an age peak at 440 to 400 Ma (Shu, 2006; Y. J. Wang and others, 2007, 2010; Shu and others, 2008b; Shen and others, 2008; F. R. Zhang and others, 2009, 2010a, 2010b; Faure and others, 2009; Z. X. Li and others, 2010; Charvet and others, 2010; Y. Zhang and others, 2011; X. B. Xu and others, 2011). Since the middle Devonian, South China has evolved into a relatively stable littoral-neritic depositional environment.

The second event was recorded by the development of a regional unconformity between middle and late Triassic strata (Shu and others, 2009). The middle Triassic uplift resulted from a collision between the south China and North China blocks, which was followed by a brittle but locally ductile folding-thrusting and a strike-slip shearing dated at 240 to 220 Ma (Charvet and others, 2010; X. B. Xu and others, 2011) as well as granitic intrusions dated at 245 to 205 Ma (Zhou and others, 2006).

The third event involved the emplacement of voluminous granitoids and acid volcanic rocks, dated at 140 to 110 Ma (D. Z. Wang and Zhou, 2002; Zhou and others, 2006; D. Z. Wang and Shu, 2012). Thus the early Paleozoic South China Fold Belt has witnessed strong reworking during the latter two events.

Polyphase Structural Deformation

The pre-Devonian rocks experienced at least two phases of ductile shearing (Charvet and others, 2010; Shu and others, 2011a). The first-phase involved coaxial pure shear under a high temperature and hydrostatic pressure condition, yielding recumbent folds with a sub-E-W axial direction, near-cylindrical folds and a symmetric augen structure within orthogneiss. A co-existing meta-rhyolite was dated at around 970 Ma (U-Pb, Shu and others, 2008c). The second-phase was characterized by non-coaxial asymmetric flexural slip folds, isoclinal folds, overturned folds and mylonitic rocks with an isotopic age in Silurian (Shu and others, 1999; Charvet and others, 2010). In fact, such kind of deformation was widely developed across the South China Fold Belt.

ANALYSES OF DEPOSITIONAL ENVIRONMENT IN THE SINIAN–EARLY PALEOZOIC PERIOD

Stratigraphic Sequences

The Upper Neoproterozoic succession.—In South China, this succession was named Sinian strata dated at 680 to 542 Ma (S. G. Zhang and Yan, 2005) and comprises slaty sandstone, siltstone and mudstone intercalated with lenticular chert or marble. The depositional thickness varies from 420 m in Jinggang, 600 m in Nanling, to 800 m in Wuyi. Rhythmic bedding, ripple marks, scour marks, graded bedding and marlite lenses are observed in the Jinggang and Nanling areas. In Jinggang and Nanling, the Sinian strata lie disconformably on the Nanhua succession that formed in the middle Neoproterozoic during regional rifting of the South China Block. The Nanhua succession contains banded iron formations and bimodal volcanic rocks (JXBGMR, 1984; J. Wang and Li, 2003).

The Lower Paleozoic succession.—Cambrian and Ordovician strata display a disconformable contact with the Sinian succession. Silurian strata are conspicuously absent in Cathaysia. The sandy-muddy strata deposited during the Cambrian-Ordovician period (up to 6000 m thick) are distributed widely in the SW Fujian, south-central Jiangxi, southern Hunan, northern Guangdong and Guangxi Provinces. The absence of volcanic or volcaniclastic rocks in the early Paleozoic rock assemblage suggests a stable depositional environment. Detailed characteristics of Cambrian and Ordovician depositional sequences are described below.

The Cambrian succession.—This succession consists of a marine sequence of metaquartz arenite, feldspathic sandstone and mudstone intercalated with bioclastic lime-

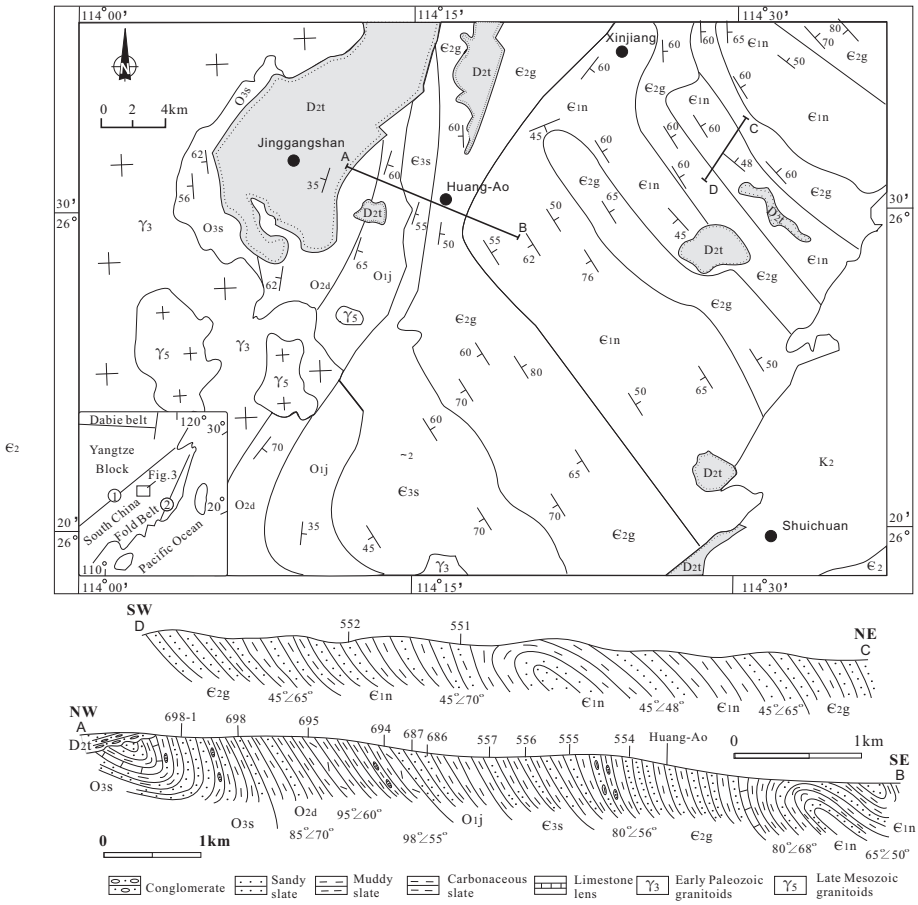

Fig. 3. Geological map in the Jinggang area with two cross-sections showing the rock assemblages and deformation features of the early Paleozoic stratigraphic sequences.

stone. Ripple mark, cross-bedding and graptolites are well preserved in the Cambrian sandstones; and trilobites and gastropods are occasionally found in the limestone. The succession is divided from bottom to top into the Niujiaohe ($\epsilon_1 n$), Gaotan ($\epsilon_2 g$) and Shuishi ($\epsilon_3 s$) formations (fig. 2B) (JXBGMR, 1984).

The Ordovician succession.—This succession includes muddy, sandy and carbonaceous rocks containing abundant graptolites along with some trilobites, corals and brachiopods. The succession was divided from bottom to top into Jueshangou ($O_1 j$), Dui'ershi ($O_2 d$), Hanjiang ($O_3 h$) and Shikou ($O_3 s$) formations (figs. 2B and 3) (JXBGMR, 1984).

Facies analysis suggests that from the early Cambrian to middle Ordovician, black shale, mudstone and carbonaceous mudstone were deposited in a deep-water environment, likely a slope setting. Exceptionally in the middle Cambrian, quartz arenite, feldspathic sandstone, intercalated limestone and quartz arenite were formed in a near-shore environment.

In the study area, the upper Ordovician Hanjiang and Shikou formations comprise lithic blocks, clastic breccia, feldspar sandstone and mudstone. The mudstone was intensely sheared and folded and contains massive sandstone blocks and angular

lithic debris. The clastic breccia consists of unsorted, angular, disorganized sandy rocks and lithic blocks with an argillaceous matrix, showing olistostrome characteristics.

Cover succession.—From the middle Devonian to early Carboniferous, conglomerate, quartz arenite, feldspathic sandstone, sandstone and siltstone intercalated with chert, limestone and bioclastic limestone were deposited unconformably on the early Paleozoic strata. During the middle Carboniferous to Permian, the depositional succession was characterized by the limestone and bioclastic limestone assemblage intercalated with coal-bearing mudstone (Shu and others, 2008a). Overall, the depositional environment for the cover succession was a littoral-neritic setting.

Sedimentary Structures and Rocks Reflecting Depositional Environments

Abundant sedimentary structures are well preserved in the Sinian to Ordovician rocks. Rhythmic bedding (fig. 4A), horizontal bedding, massive bedding (>1 m thickness), cross-bedding and wavy scour mark are the principal sedimentary structures. Occasionally, rounded load marks and elliptical flute casts are found to co-exist with the above structures. Ripple mark (fig. 4B), load mark (fig. 4C), lenses (fig. 4D), cross-bedding (fig. 4E), ripple cross-lamination and flaser bedding are mainly developed in the sandy rocks of the middle Cambrian and upper Ordovician, indicating a littoral-neritic depositional environment.

A massive olistostrome structure, in which sandstone blocks (fig. 4F) from meter-scale up to 180 m × 60 m are embedded in a siltstone and mudstone matrix, was observed in the late Ordovician succession in the Jinggang and Nanling areas (Rong and others, 2010; X. Chen and others, 2010, 2012).

Based on the field investigations, the following lithologic associations were recognized: (1) quartz arenite interbedded with carbonaceous rock (fig. 4G), (2) bioclastic limestone intercalation (fig. 4H), containing coral and brachiopod fossils, suggesting a neritic environment, and (3) olistostrome only developed in the upper Ordovician (Shu and others, 2008b). We have not found any typical turbidite with the Bouma sequence.

Based on the above sedimentary structures, a littoral-neritic depositional setting is inferred to have prevailed in the early Cambrian, middle Cambrian and late Ordovician periods, whereas a neritic-bathyal setting dominated during the late Cambrian to middle Ordovician. The late Ordovician is likely a transitional period from bathyal to littoral-land environment related to the initial uplift. This is supported by the late Ordovician depositional sequence consisting of large angular masses and coarser clastic rocks.

Paleo-Current Direction

In South China, fresh outcrops are rare due to intense weathering and vegetation; therefore, sedimentary structures with paleocurrent indicators are difficult to find. Nevertheless, we obtained 74 measurements (figs. 5A-5F) on crossbeds from the early Paleozoic sedimentary rocks; 46 measurements from the South China Fold Belt, and 28 from Jiangnan.

The rose diagrams of 25 measurements from the Jinggang area display a prevailing direction of 285° to 300° (figs. 5A and 5B) for the middle Cambrian paleocurrents. The 12 measurements for the late Ordovician rocks from the Nanling area gave a prevailing direction of 295° (fig. 5C), and 9 measurements for the middle Cambrian rocks from the western Wuyi area gave the maximum value toward 348° (fig. 5D). A few measurements for early Cambrian rocks from the northern Jinggang yielded southward paleocurrents.

In the southern Jiangnan belt, 28 measurements for the late Ordovician sandstones show a prevailing direction of 320° (figs. 5E and 5F).

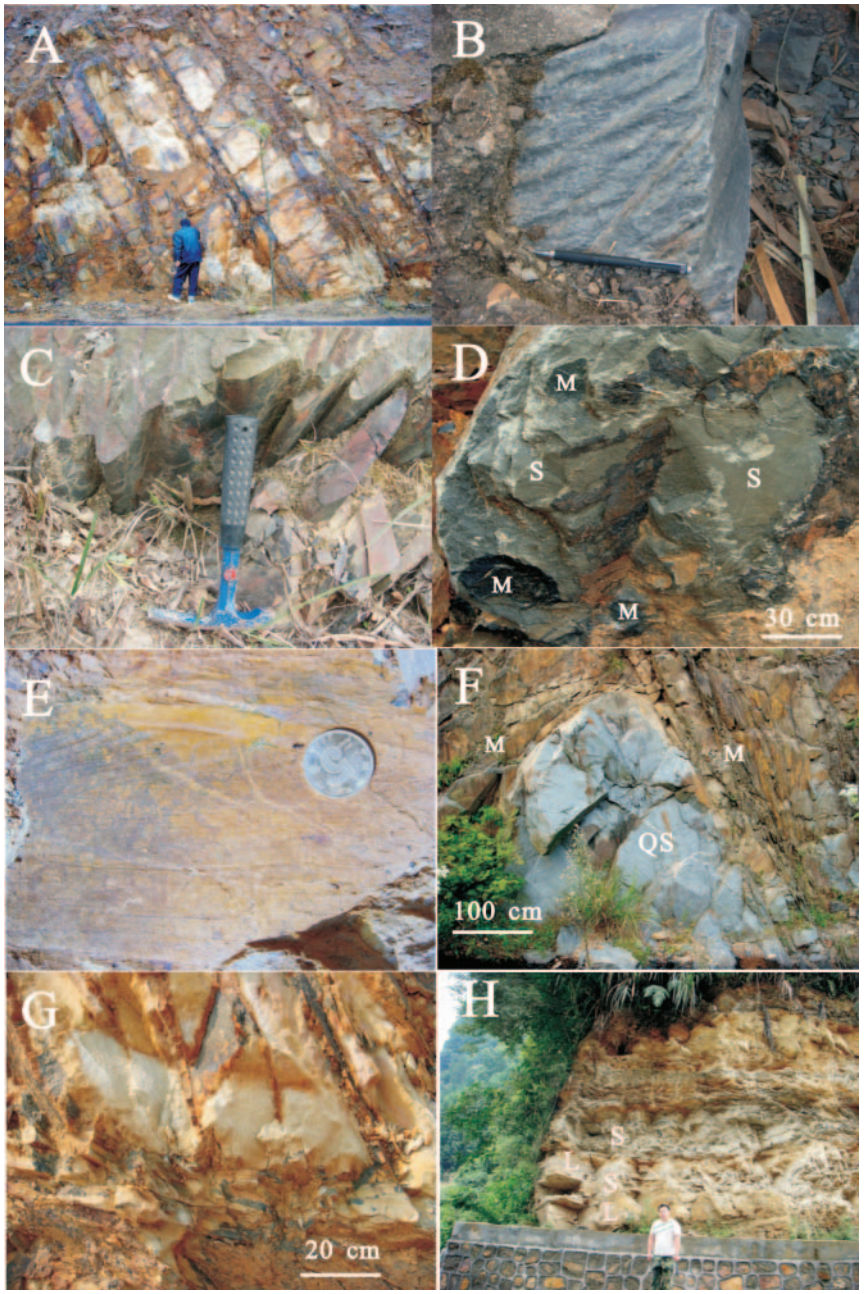

Fig. 4. Sedimentary structures and rocks reflecting depositional environments during early Paleozoic in the Jinggang and Nanling areas. (A) Interbedded sandstone and mudstone (lower Cambrian); (B) ripple marks in the sandstone (lower Cambrian); (C) flute cast of sandstone (upper Cambrian); (D) lenticular mudstone masses in sandstone (upper Cambrian); (E) cross-bedding in the siltstone (middle Ordovician); (F) big quartz arenite mass wrapped by mudstone (upper Ordovician); (G) feldspar sandstone with oblique bedding (upper Cambrian); (H) intercalated limestone layers in the sandstone (lower Cambrian). S, Sandstone; M, mudstone; L, limestone; QS; quartz sandstone.

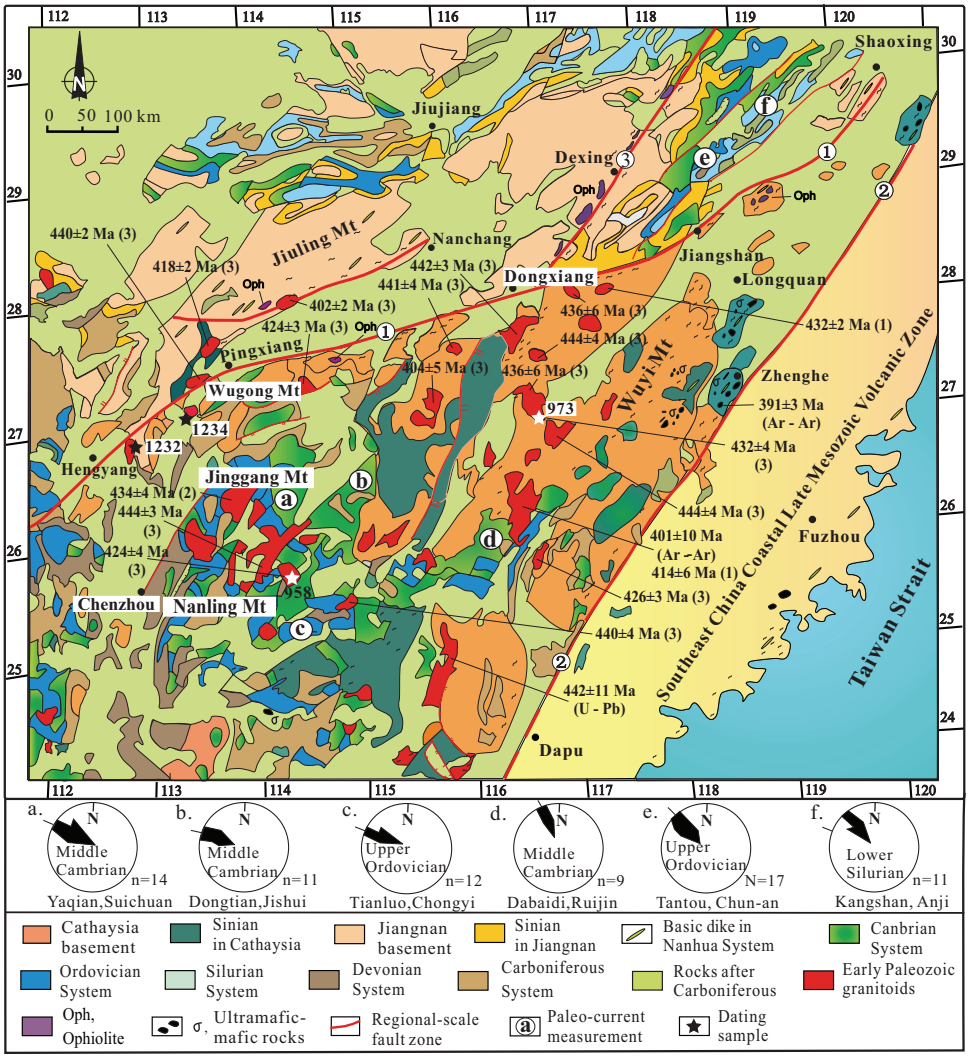

Fig. 5. Geological map showing the distribution of early Paleozoic granites with isotopic dating data and the paleo-current direction. ①, Shaoxing-Jiangshan-Pingxiang fault zone; ②, Zhenghe-Dapu fault zone; ③, Dongxiang-Dexing fault zone; Numbers in brackets show the isotopic dating methods: 1, SHRIMP zircon U-Pb; 2, SIMS zircon U-Pb; 3, LA-ICPMS zircon U-Pb. The GPS *coordinates* of sampling: sample 973, N25°49.440′, E114°24.817′ (Doushui); sample 958, N27°11.118′, E116°43′206′ (Lichuan); sample 1232, N27°12.035′, E112°58′820′ (Hengdong) and sample 1234, N27°12.045′, E112°58′839′ (Zhenzhu).

The paleocurrent data suggest that the source for the early Paleozoic sedimentary rocks in the South China Fold Belt, as well as in the southern Jiangnan belt, lay to the east and southeast. Crossbed data from the Sinian sandstones are limited but roughly indicate a sediment transport northwestward.

A Comparison of Stratigraphic Sequences between the Jiangnan, Cathaysian Domains and their Transitional Zone

The Neoproterozoic strata in the Jiangnan domain are composed of clastic rocks intercalated with bimodal volcanic rocks, tillites, siliciclastic rocks and carbonate rocks

(limestone and dolomite). In contrast, the coeval stratigraphic sequence in the Cathaysia domain is an association of meta-sandstone, siltstone and mudstone intercalated with lenticular limestone. Tillite and carbonate rock are rare. Rhythmic bedding and graded bedding occur widely in the Neoproterozoic sequence. In the transitional zone between the depositional domains of Jiangnan and Cathaysia, the Neoproterozoic carbonate rocks decrease whereas the clastic components increase, although the tillites in the late Nanhua rift succession are well developed.

The Cambrian strata in the Jiangnan domain consist of coal-bearing carbonaceous and trilobite- and *Sinoceras-bearing* carbonate rocks. In contrast, feldspathic sandstone and mudstone are the main constituents of the Cambrian strata in Cathaysia. The main rock assemblages in the transitional zone are carbonate rocks, sandstone and mudstone.

In the Ordovician, the Jiangnan domain is mainly composed of fossil-rich carbonates and flysch. However, the coeval depositional sequence in Cathaysia mainly comprises rhythmic sandy and muddy rocks intercalated with limestone lenses. A set of carbonate, muddy and sandy rocks are preserved in the transitional zone (fig. 2).

A marked difference exists between the Jiangnan and Cathaysia domains in the Silurian. In Jiangnan, the stratigraphic sequence consists of sandstone and mudstone, in which rhythmic and micro-bedding are well preserved (fig. 2A). However, the Silurian strata are absent in Cathaysia (fig. 2B). Contemporaneous stratigraphic sequences in the transitional zone are mainly composed of coarse-grained arenite and quartz sandstone (fig. 2C), which were sourced from Cathaysia.

ANALYTICAL METHODS

Major and Trace Elements

The major element contents were analyzed by XRF method in the Modern Analysis Center of Nanjing University. Trace element abundances (including REE) were determined using a Finnigan MAT Element II-type ICP-MS in the State Key Laboratory for Mineral Deposits Research, Nanjing University. The working conditions and procedures are same as those described by Rickwood (1989), Qi and Gregoire (2000), and Qi and others (2000). The uncertainties reported in this study are 2 percent for major elements (XFR), and 5 percent for trace elements (ICP-MS).

Sm-Nd Isotopic Compositions

The Sm-Nd isotopic compositions were analyzed using a MAT-262 mass spectrometer in the Isotope Laboratory of Geology and Geophysics Institute, Academia Sinica, Beijing. Sm and Nd concentrations were determined by the isotope dilution method. During the mass analysis, $^{143}Nd/^{144}Nd$ ratios were normalized to $^{146}Nd/^{144}Nd$ (0.7219) for mass discrimination correction. Analyses of rock standards BCR-2 yielded $^{143}Nd/^{144}Nd = 0.512636 \pm 10$ (2 sigma-mean) for BCR-2, and 0.512112 ± 11 (2 sigma-mean) for JNdi-1. The total blanks for Sm and Nd of the whole analytical procedure are 5×10^{-11}g for both Sm and Nd.

Zircon U-Pb Geochronology

Zircon U-Pb isotopic compositions were analyzed at the State Key Laboratory for Mineral Deposits Research, Nanjing University. A laser spot size of 30 μm in diameter and a 5 Hz repetition rate were used for all analyses. The U-Pb fractionation was corrected using zircon standard GEMOC GJ-1 ($^{207}Pb/^{206}Pb$ age of 608.5 ± 1.5 Ma) (Jackson and others, 2004) and accuracy was determined using zircon standards Mud Tank (intercept age of 732 ± 5 Ma (Black and others, 2003). The work process was performed according to the procedure described by Compston and others (1992) and X. L. Wang and others (2007). U-Th-Pb age calculations and construction of concordia diagrams were performed using the ISOPLOT/Ex software (ver. 2.49) (Ludwig, 2001).

In Situ Lu–Hf Isotopic Compositions

In situ Lu–Hf isotope analyses were performed on the same spots of zircon grains subjected to the U–Pb dating at the State Key Laboratory of Continental Dynamics, Northwest University, Xi'an. A Nu Plasma MC-ICP-MS was used with a Geolas CQ 193 nm ArF excimer laser ablation system. The instrumental parameters are: 1300 w for power; Nebulizer gas, 0.1 m L/min; Auxiliary gas, 0.8 L/min; Plasma gas, 13 L/min. The American standard samples (MON-1, GJ-1, 91500) were used to monitor the quality of the samples (external standard). Internal standard had not been set due to a small effect on the Hf isotopic composition during the analyses. The beam diameter was 44 μm under 8 Hz and 400 shots. The analytical procedures are similar to those described by Yuan and others (2008). The two-stage model age (T_{DM2}) was calculated for the source rock of magma using $^{176}Lu/^{177}Hf = 0.015$ for the average continental crust (Griffin and others, 2002), two-stage model ages (T_{DM2}) relative to average continental crust were chosen when $\varepsilon_{Hf}(t)$ values are negative.

FINGERPRINTS OF TECTONIC SETTING FROM GEOCHEMISTRY OF SEDIMENTARY ROCKS

Geochemical Characterization and Provenance of the Early Paleozoic Sediments

Sampling.—In order to understand the compositions and tectonic settings of the sedimentary rocks, 12 rock samples from the Jinggang area (fig. 3) were analyzed for geochemical and Sm-Nd isotopic compositions, including six from Cambrian strata and six from Ordovician sequence. All samples are fresh with no fracturing or alteration. The analytical results are listed in tables 1 and 2.

Chemical characteristics of sediments.—Integrating data on the framework composition of the sandstones with SiO_2 and Al_2O_3 contents (Bhatia, 1983), four types of clastic rocks can be distinguished from the twelve samples analyzed. These are quartz-sandstone (quartz ~90%, feldspar 5-8%, lithic grains 3-5%; high-Si, low-Al), feldspathic sandstone (quartz 50-65%, feldspar 20-25%, lithic grains 5-8%; lower-Si and higher-Al), graywacke (quartz 30-40%, feldspar 8-10%, lithic grains 55-65%; high-Fe, Mg and low-K) and sandstones or lithic feldspar sandstones (quartz 50-55%, feldspar 30-35%, lithic grains 15-20%) (table 1).

On tectonic setting discrimination diagrams (fig. 6), all Cambrian samples plot in the field of passive continental margin, whereas six samples of the Ordovician rocks plot in three fields of passive margin (dominant), active margin (fig. 6A) and continental island arc (figs. 6A and 6B). These results suggest a complex provenance, implying derivation from the Proterozoic volcanic rocks of island arc (compare, Shu, 2006; Shu and others, 2011a).

The ratio between strongly incompatible (La, Th, Zr) and compatible (Sc) elements is considered to reflect the provenance and tectonic setting (Bhatia and Taylor, 1981; Bhatia, 1983, 1985; Bhatia and Crook, 1986). The ratios Rb/Sr, Ba/Sr, Th/U, Zr/Y, La/Sc, Th/Sc and Sc/Cr derived from Cambrian and Ordovician rocks define a provenance of stable depositional environment. In the (La/Th) versus Hf plot (table 3) (fig. 7), most samples fall in the field of felsic source in upper crust whereas Sample 556 from the upper Cambrian plots in the field of mixed felsic-basic source.

As shown in the upper-crust-normalized spidergrams (fig. 8A) (Taylor and McLennan, 1985), all samples show similar features. Spidergrams with distinct Ba, Nb, Sr and P negative anomalies, seem to be typical of sedimentary rocks derived from upper crustal source. In figure 8B, all the sandstone samples have rather similar REE patterns: LREE-enriched (LREE/HREE = 7.7 − 15.4 and (La/Yb)n = 14 − 41) with negative Eu anomalies (Eu/Eu* = 0.56 − 0.68, average 0.60). Combined with the field observations, the Cambrian and Ordovician clastic rocks were likely deposited in a neritic to bathyal setting without remarkable input of mantle-derived compositions.

TABLE 1

Major (wt %) and trace ($\times 10^{-6}$) element data of sedimentary rocks from the Jinggangshan domain

Sample	**551**	**552**	**554**	**555**	**556**	**557**	**686**	**687**	**694**	**695**	**698**	**698-1**
Stratum	Lower Cambrian		Middle Cambrian		Upper Cambrian		Lower Ordovician		Middle Ordovician		Upper Ordovician	
Rock	LFS	Quartz-sandstone			Feldspar sandstone				Graywacke		LFS	
SiO_2	73.84	89.31	90.63	89.12	69.46	71.27	71.29	70.43	68.38	66.72	79.51	79.73
TiO_2	0.43	0.51	0.45	0.47	0.45	0.40	0.33	0.36	0.62	0.65	0.31	0.35
Al_2O_3	15.97	3.58	3.85	5.38	19.43	18.06	17.02	18.85	17.67	18.65	9.98	10.15
TFeO	3.07	2.65	1.92	1.94	2.25	2.8	3.15	3.01	5.26	5.23	3.65	3.52
MnO	0.11	0.05	0.13	0.21	0.12	0.12	0.04	0.05	0.1	0.13	0.05	0.13
MgO	0.07	0.16	0.09	0.83	0.52	0.22	0.98	0.95	2.19	2.63	0.66	1.09
CaO	0.32	0.29	0.16	0.25	0.29	0.27	0.75	0.06	1.38	1.05	0.29	0.16
Na_2O	1.54	0.85	0.74	0.49	1.96	1.78	1.66	1.59	2.06	2.15	1.25	1.24
K_2O	2.74	1.47	1.66	1.17	3.45	3.17	2.68	2.95	0.95	1.33	2.07	2.06
P_2O_5	0.13	0.11	0.08	0.08	0.12	0.09	0.12	0.13	0.07	0.12	0.11	0.08
LOI	1.55	0.94	0.64	0.68	1.76	2.11	2.01	1.38	2.1	2.05	1.94	2.04
Total	99.77	99.92	100.35	100.62	99.81	100.29	100.03	99.76	99.68	100.11	99.82	100.55
Sc	8.19	6.68	6.83	7.39	7.38	6.56	8.62	8.05	7.73	7.42	8.23	8.5
V	110.45	82.51	60.86	67.02	148.24	145.19	541.7	78.58	152.88	148.65	179.2	157.3
Cr	58.88	28.19	33.73	35.02	46.12	41.36	37.67	39.62	44.69	42.71	43.79	43.39
Rb	228.7	185.1	129.2	118.8	186.6	190.6	115.5	131.1	192	199.2	235.1	227.6
Sr	40.98	10.03	48.42	30.65	63.75	48.06	34.6	29.86	20.14	48.29	26.81	22.78
Y	12.3	11.2	9.7	13.8	14.3	13.2	22.1	21.4	13.2	18.2	18.4	11.3
Zr	238.6	276.2	273.2	282.2	266.5	315.4	270.3	286.4	230.4	232.6	258.8	195.3
Cs	13.21	8.65	7.756	8.15	10.32	12.34	8.12	7.33	13.135	15.54	11.23	10.56
Ba	468.3	425	393.1	497.2	441.7	483.6	520.4	645.4	468.5	614.6	736	634.5
Hf	5.86	4.68	5.83	4.78	3.88	4.92	6.07	6.49	4.28	5.72	3.79	6.12
Th	25.78	21.76	22.68	24.26	18.39	19.82	21.63	28.288	23.383	26.58	25.96	24.67
U	2.44	1.87	1.73	1.92	2.36	2.62	2.38	2.38	3.168	2.69	4.11	4.13
La	101.25	95.28	58.86	92.06	89.93	89.47	105.53	96.58	69.57	61.39	97.55	85.31
Ce	120.2	72.01	55.63	77.12	75.00	108.8	124.9	92.12	88.21	115.8	113.9	112.8
Pr	11.32	8.60	6.62	10.83	8.07	12.35	18.13	10.14	15.73	12.54	16.68	15.28
Nd	40.64	33.88	26.31	42.62	31.91	45.33	85.06	43.89	58.59	45.49	71.81	56.41
Sm	7.46	5.67	4.19	7.71	4.96	7.59	17.81	7.09	9.87	7.69	12.42	10.60
Eu	1.36	1.04	0.79	1.50	0.95	1.41	3.95	1.47	1.98	1.54	2.22	1.86
Gd	6.86	5.14	3.82	7.62	4.72	6.92	17.04	7.12	9.83	7.13	10.75	9.52
Tb	1.00	0.78	0.57	1.08	0.71	0.97	2.47	1.07	1.45	1.04	1.53	1.48
Dy	5.58	4.31	3.15	5.73	4.08	4.98	12.49	5.97	7.90	5.54	8.22	8.20
Ho	1.01	0.77	0.56	0.99	0.78	0.84	1.95	1.08	1.41	0.99	1.44	1.46
Er	2.97	2.30	1.72	2.90	2.36	2.37	4.94	3.27	4.12	2.90	4.47	4.46
Tm	0.42	0.34	0.24	0.38	0.34	0.33	0.76	0.46	0.57	0.42	0.61	0.60
Yb	2.71	2.20	1.56	2.47	2.17	2.21	4.38	3.01	3.51	2.72	3.85	3.83
Lu	0.41	0.34	0.23	0.38	0.33	0.34	0.66	0.45	0.52	0.41	0.59	0.58
∑REE	282.2	232.66	194.21	263.39	226.31	283.91	375.87	273.11	273.26	265.6	372.04	322.39
L/H	12.5	13.4	15.4	11.2	13.6	14.0	7.7	11.2	8.3	11.6	10.8	9.7
$(La/Yb)_N$	26.5	31.1	40.8	29.6	29.7	29.0	17.6	22.9	14.2	16.2	16.7	16.0
δEu	0.57	0.58	0.59	0.59	0.59	0.58	0.68	0.63	0.61	0.62	0.57	0.56
δCe	0.99	0.92	0.95	0.76	0.99	0.94	0.90	1.00	0.64	0.99	0.79	0.92
Rb/Sr	5.6	8.5	2.7	3.9	2.9	4.0	3.3	4.4	9.5	1.8	8.8	10.0
Ba/Sr	13.9	12.4	8.1	16.2	6.9	10.1	7.0	21.6	23.3	5.7	27.5	27.9
Th/U	10.6	11.6	13.1	12.6	7.8	7.6	9.1	11.9	7.4	9.9	6.3	6.0
Zr/Y	19.4	24.6	28.1	20.4	18.6	23.9	12.2	13.4	17.4	12.8	14.1	17.3
La/Sc	12.2	14.3	13.0	13.8	12.2	13.6	9.6	11.9	9.0	8.3	10.9	10.0
La/Th	3.9	4.4	3.9	4.2	4.9	4.5	3.8	3.4	3.0	2.3	3.4	3.5
Th/Sc	3.1	3.3	3.3	3.3	2.5	3.0	2.5	3.5	3.0	3.6	3.2	2.9
Sc/Cr	0.14	0.24	0.20	0.21	0.16	0.16	0.23	0.20	0.17	0.17	0.19	0.20

Notes: LFS, Lithic feldspar sandstone; TFeO = FeO + Fe_2O_3.

TABLE 2

Sm-Nd isotope compositions in the Early Paleozoic sedimentary sequences in the SCFB

Sample	Stratum	$t_{Str.}$ (Ma)	Sm (10^{-6})	Nd (10^{-6})	$^{147}Sm/^{144}Nd$	$(^{143}Nd/^{144}Nd) \pm 2\sigma(\times10^{-6})$	$\varepsilon_{Nd}(t)$	t_{DM} (Ma)
698-1	Upper	455	9.287	52.06	0.1079	0.511733±14	-12.5	2204
698	Ordovician	455	4.513	24.43	0.1117	0.511759±10	-12.2	2181
695	Middle	470	2.438	13.82	0.1066	0.511857±13	-7.9	2042
694	Ordovician	470	2.776	15.04	0.1116	0.511846±12	-10.4	2042
687	Lower	480	3.965	21.88	0.1096	0.511840±11	-10.2	2041
686	Ordovician	480	6.524	35.77	0.1103	0.511831±10	-10.5	2059
557	Upper	495	8.588	45.92	0.1131	0.511695±11	-13.1	2285
556	Cambrian	495	17.11	75.26	0.1374	0.511907±13	-10.5	2077
555	Middle	510	5.225	28.04	0.1127	0.511658±11	-13.7	2342
554	Cambrian	510	5.954	30.25	0.1190	0.511668±8	-13.9	2360
552	Lowe	530	9.963	53.28	0.1128	0.511628±12	-13.6	2348
551	Cambrian	530	9.943	55.04	0.1092	0.511722±12	-12.0	2220

Notes: t, age; $t_{Str.}$, deposition age after from Zhang and Yan, 2005. The Nd isotope model ages (t_{DM}) are calculated by two-stage model whose equation and related parameter values are as follows: $t_{DM}=1/\lambda \cdot \ln\{1 + [(^{143}Nd/^{144}Nd)_m(^{143}Nd/^{144}Nd)_{DM} - [(^{147}Sm/^{144}Nd)_m - {}^{147}Sm/^{144}Nd)_C](e^{\lambda t} - 1)]/[(^{147}Sm/^{144}Nd)_C - (^{147}Sm/^{144}Nd)_{DM}]\}$, of them, $^{147}Sm/^{144}Nd)_C = 0.118$, $(^{143}Nd/^{144}Nd)_{DM} = 0.513151$, $(^{147}Sm/^{144}Nd)_{DM} = 0.2136$.

Sm-Nd isotopes.—Twelve samples were analyzed for Nd isotopic compositions. As shown in table 2 (see also footnote of this table regarding data corrections), all the samples show negative $\varepsilon_{Nd}(t)$ values (−7.9 to −13.9) and two-stage model ages range from 2042 to 2360 Ma. In the $\varepsilon_{Nd}(t) - T_{str}$ diagram (fig. 9), the rocks plot in the field of Paleoproterozoic crustal evolution of the South China Craton (Shen and others, 1993; Hu and Zhang, 1998), suggesting their ultimate derivation from Paleoproterozoic continental crust.

THE EARLY PALEOZOIC TECTONO-MAGMATIC EVENT

Structural Deformation

A regional-scale tectono-magmatic event took place in Cathaysia in Silurian. This event included folding (fig. 3), thrusting and large-scale anatexis with granite emplace-

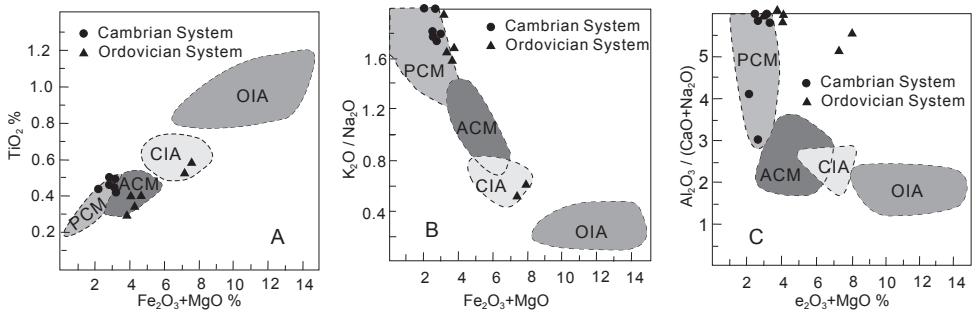

Fig. 6. Major element composition plots of sandstones for tectonic setting discrimination (after from M. R. Bhatia, 1983). OIA, Oceanic island arc; CIA, Continental island arc; ACM, Active continental margin; PCM, Passive continental margin.

TABLE 3

Average ratios of element pair of sandstone in various tectonic settings

Ratio	Oceanic arc*	Continental arc*	Active continental margin*	Passive continental margin*	Cambrian System in the SCFB (6)	Ordovician System in the SCFB (6)
Rb/Sr	0.05	0.65	0.89	1.19	4.6	6.3
Ba/Sr	0.95	3.55	3.8	4.7	6.9	18.8
Th/U	2.1	4.6	4.8	5.6	10.6	8.4
Zr/Y	5.7	9.6	7.2	12.4	22.5	14.5
La/Sc	0.55	1.82	4.55	6.25	13.2	10.0
Th/Sc	0.15	0.85	2.59	3.06	3.1	3.1
Sc/Cr	0.57	0.32	0.30	0.16	0.19	0.2

* Bhatia and others, 1986; the number within bracket, sample numbers in this study.

ment and lower greenschist facies metamorphism. The axial trends of the folds are variable, and the predominant axial directions are sub-E-W and NE-trending. A shortening up to 67 percent has been measured from the folded strata (Shu and others, 2008b). Strong folding was commonly accompanied by regional-scale thrusting and ductile shearing, which characterize the major structural fabric of the South China Fold Belt.

Taking the Wuyi Mountains as an axial zone of the ductile deformation domain, the kinematic indicators (shearing foliation, stretching lineation and various asymmetric fabrics) reveal a fan-shaped ductile thrusting pattern in a geological cross-section across the Cathaysia block (see below). A top-to-the-southeast thrust occurs in the southeastern Cathaysia (Faure and others, 2009; Charvet and others, 2010) and a top-to-the-northwest thrust took place in the Jinggang segment (Shu and others, 2008b; Charvet and others, 2010), both of which were reworked by a late strike-slip shearing. Locally, northward down-slip structures were observed on the northern side of the syntectonic granitic doming. The ^{40}Ar-^{39}Ar analyses of neo-formed muscovite

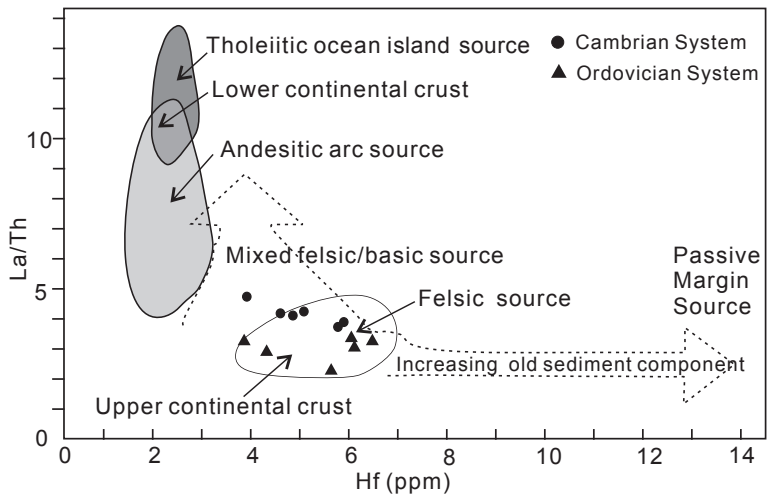

Fig. 7. The (La-Th)-Hf diagram for provenance discrimination.

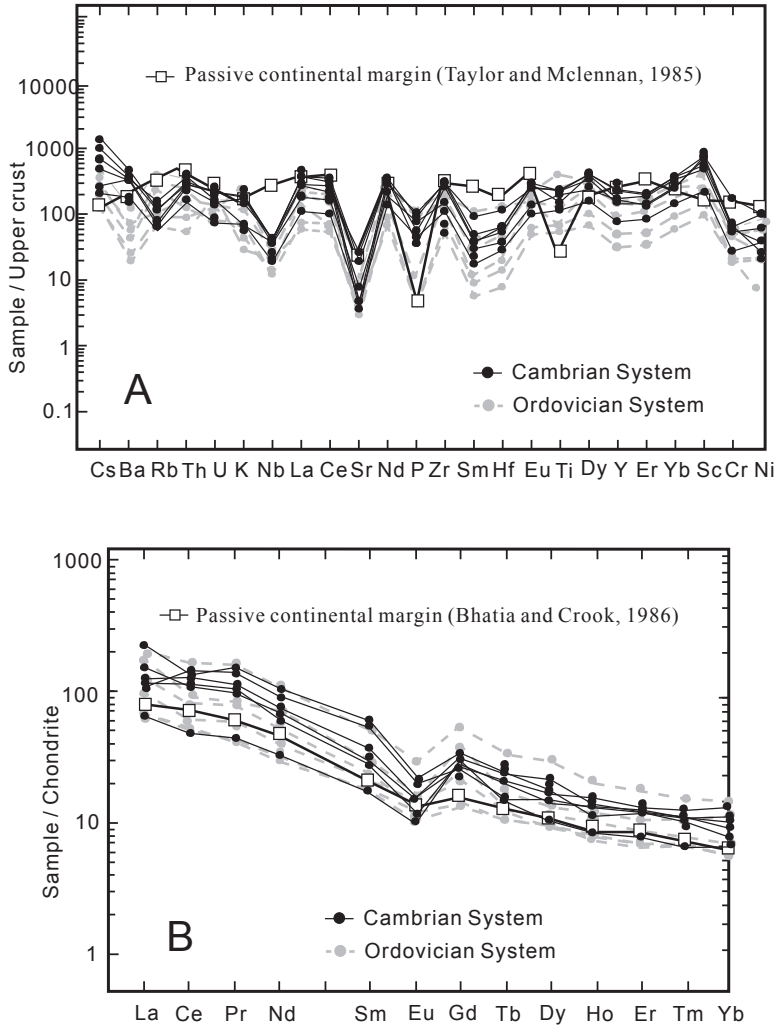

Fig. 8. Distribution of (A) trace elements and (B) rare earth elements for the sandstones derived from the Jinggang area.

and biotite from mylonitic rocks defined an age range of 430 to 390 Ma (Shu and others, 1999, 2008b; Y. J. Wang and others, 2007, 2010; Faure and others, 2009; Charvet and others, 2010; X. B. Xu and others, 2011; Y. Zhang and others, 2011). Strong northwestward thrusting led to the development of the Silurian foreland that was followed by a northwestward closure of the marine basins through the late Ordovician-early Devonian period (Rong and others, 2003, 2010).

The Early Paleozoic Granitic Magmatism

Sampling from representative plutons.—Granitic plutons occur widely in the South China Fold Belt, covering an area of 20,000 km^2. The early Paleozoic granites were first reported in South China by K. Q. Xu and others (1960, 1963), but reliable isotopic ages for these granitoids were scarce until 1990's.

Four muscovite-bearing granitic plutons (Doushui, Lichuan, Hengdong and Zhenzhu) occur in the Nanling and Wuyi segments of the South China Fold Belt (fig.

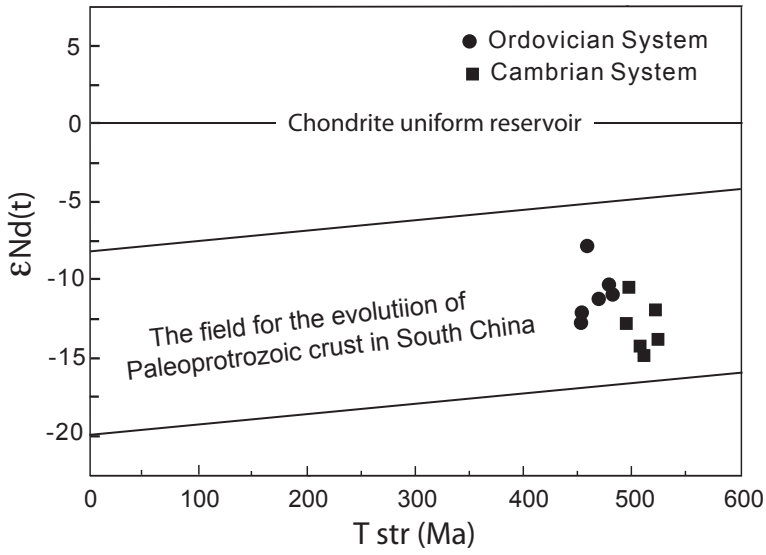

Fig. 9. The $\varepsilon_{Nd}(t)$ vs. T_{str} diagram, suggesting a continental crustal source.

5). These plutons intrude Cambrian-Ordovician strata and show porphyritic and augen textures. The major phases comprise K-feldspar (15-20%), quartz (10-15%) and mica (5-10%), and a medium-to-fine-grained groundmass (quartz, microcline, albite, biotite and muscovite, total 65-70%). They have not been precisely dated, even though early Paleozoic ages have been assigned from the inference of middle Devonian fossils in the overlying sedimentary rocks. We therefore carried out a LA-ICP-MS zircon U-Pb dating and *in situ* Hf isotopic analysis on the four granite plutons. The sampling locations are shown in figure 5. The analyzed results of zircon U-Pb dating are listed in table 4.

Geochronological results.—Sample 973 was collected from the Lichuan foliated muscovite-bearing granite in the western Wuyi Mts. Zircon grains separated from this sample are euhedral and prismatic with clear oscillatory zoning as well as the high Th/U ratios (from 0.12 to 0.57), indicative of magmatic origin. 20 analyses with discordance within ±10 percent yield a weighted mean $^{206}Pb/^{238}U$ age of 434.8 ± 4.1 Ma (MSWD = 2.0; fig. 10A). This age is considered to represent the crystallization age of this rock.

Sample 958 was collected from the Doushui massive muscovite-bearing granite in the Nanling Mts. The similar magmatic features are also displayed in zircon grains from this sample. Seventeen analyses gave a weighted mean $^{206}Pb/^{238}U$ age of 424.1 ± 5.2 Ma (MSWD = 4.9; fig. 10B).

Sample 1232 is a porphyritic biotite granite collected from Hengyang in the northern Nanling Mountains. This pluton was once considered as an early Cretaceous age (HNBGMR, 1987). Zircons of sample are prismatic with high Th (129-468 ppm) and U (83-213 ppm), and high Th/U ratios (from 0.82-4.57), suggesting a magmatic origin. 24 concordant ages yield a weighted mean $^{206}Pb/^{238}U$ age of 428.1 ± 2.5 Ma (MSWD = 0.82; fig. 10C). This age is interpreted as the crystallization age of this rock.

Sample 1234 was collected from the Zhenzhu massive biotite granite that is located ~100 km to the northeast of Hengyang City. Zircon grains separated from sample 1234 are euhedral and prismatic with oscillatory zoning and very higher Th/U

TABLE 4

Analytical results of LA ICPMS zircon U-Pb dating for four granitic plutons in the South China Fold Belt

Spots	Isotopic ratios			Age/Ma (±1σ)			Th/U
	$^{207}Pb/^{206}Pb\pm1\sigma$	$^{207}Pb/^{235}U\pm1\sigma$	$^{206}Pb/^{238}U\pm1\sigma$	$^{207}Pb/^{206}Pb$	$^{207}Pb/^{235}U$	$^{206}Pb/^{238}U$	
Sample 973: GPS N27°11.118'. E116°43'206'. Lichuan Granite. 434.8 ± 4.1 Ma (n=20)							
973-1	0.05608±0.00156	0.54025±0.01482	0.06989±0.00104	456±35	439±10	435±6	0.57
973-2	0.05557±0.00117	0.51712±0.01102	0.0675±0.00092	435±25	423±7	421±6	0.43
973-3	0.05535±0.00162	0.52926±0.01544	0.0694±0.00115	426±36	431±10	433±7	0.16
973-4	0.05572±0.00125	0.52936±0.01182	0.06891±0.00094	441±27	431±8	430±6	0.53
973-5	0.05619±0.00138	0.54093±0.01333	0.06983±0.00099	460±30	439±9	435±6	0.44
973-6	0.05695±0.00141	0.54687±0.0138	0.06969±0.0011	490±29	443±9	434±7	0.12
973-7	0.05814±0.00125	0.54631±0.0122	0.06819±0.00103	535±25	443±8	425±6	0.05
973-8	0.05547±0.00127	0.51214±0.01192	0.067±0.00097	431±27	420±8	418±6	0.60
973-9	0.05584±0.00165	0.52972±0.01386	0.06881±0.00094	446±67	432±9	429±6	0.13
973-10	0.12569±0.00278	4.55286±0.09996	0.26283±0.00386	2039±20	1741±18	1504±20	0.55
973-11	0.05615±0.00117	0.54101±0.0117	0.06989±0.001	458±24	439±8	435±6	0.15
973-12	0.05556±0.00175	0.54834±0.01712	0.07163±0.0012	435±40	444±11	446±7	0.30
973-13	0.0566±0.00124	0.55637±0.01275	0.07133±0.00109	476±26	449±8	444±7	0.18
973-14	0.05578±0.00125	0.54346±0.01249	0.07067±0.001	444±27	441±8	440±6	0.67
973-15	0.05746±0.00151	0.53867±0.01437	0.06812±0.00117	509±30	438±9	425±7	0.14
973-16	0.05709±0.00121	0.57566±0.01254	0.07314±0.00101	495±25	462±8	455±6	0.61
973-17	0.05619±0.00121	0.54995±0.01202	0.071±0.00097	460±26	445±8	442±6	0.44
973-18	0.1586±0.00161	6.9091±0.07338	0.31606±0.00463	2441±12	2100±9	1770±23	0.18
973-19	0.05707±0.00109	0.5541±0.01034	0.07043±0.00104	494±19	448±7	439±6	0.53
973-20	0.05599±0.00068	0.54127±0.00656	0.07012±0.00091	452±13	439±4	437±5	0.20
973-21	0.05579±0.00215	0.53899±0.01999	0.06808±0.00159	444±53	444±53	437±7	0.5
973-22	0.056±0.00205	0.54459±0.01937	0.06882±0.00144	452±49	452±49	439±7	0.31
Sample 958: N25º49.440'. E114º24.817'. Doushui Granite. 424.1 ± 5.2 Ma (n=17)							
958-1	0.05603±0.00076	0.51954±0.00773	0.06729±0.00084	443±18	439±6	438±5	0.43
958-2	0.18223±0.00247	0.67523±0.01419	0.42523±0.00057	2673±23	2495±12	2283±26	1.1
958-3	0.07043±0.00112	1.51768±0.02370	0.15634±0.00213	941±33	938±10	936±12	1.4
958-4	0.05648±0.00105	0.50441±0.00910	0.06491±0.00132	471±42	415±6	405±6	0.37
958-5	0.05607±0.00113	0.50267±0.00973	0.06514±0.00138	455±46	414±7	407±6	0.46
958-6	0.05355±0.00078	0.49163±0.00712	0.06663±0.00091	352±34	406±5	416±5	1.09
958-7	0.06158±0.00196	0.52631±0.01705	0.06552±0.00108	660±70	449±11	409±7	0.47
958-8	0.05548±0.00116	0.49865±0.01012	0.06523±0.00109	432±48	411±7	407±6	0.49
958-9	0.05564±0.00103	0.52483±0.00937	0.06843±0.00106	438±42	428±6	427±6	0.51
958-10	0.05860±0.00087	0.55042±0.00804	0.06816±0.00093	552±33	445±5	425±5	0.53
958-11	0.05655±0.00113	0.51614±0.01031	0.06622±0.00104	474±45	423±7	413±6	0.72
958-12	0.05744±0.00119	0.52642±0.01061	0.06651±0.00092	508±47	429±7	415±6	1.02
958-13	0.06712±0.00162	1.27681±0.02943	0.13806±0.00213	841±51	835±13	834±12	1.08
958-14	0.05499±0.00072	0.51113±0.00661	0.06742±0.00093	412±30	419±4	421±5	0.39
958-15	0.05547±0.00076	0.53621±0.0073	0.07012±0.00093	431±14	436±5	437±6	0.16
958-16	0.05572±0.00125	0.50936±0.01182	0.06891±0.00094	441±27	431±8	430±6	0.53
958-17	0.05536±0.00135	0.5426±0.01321	0.07112±0.001	427±30	440±9	443±6	0.19
958-18	0.05578±0.00125	0.54346±0.01249	0.07067±0.001	444±27	441±8	440±6	0.67
958-19	0.0554±0.00084	0.53565±0.00798	0.07014±0.00093	428±15	436±5	437±6	0.96
958-20	0.05547±0.00112	0.52072±0.00908	0.06795±0.0011	431±24	431±24	434±6	0.14
Sample 1232: N27°12.035'. E112°58'820'. Hengdong Granite. 428 ± 3 Ma (n=24)							
1232-01	0.05634±0.00123	0.52343±0.01185	0.06739±0.00098	466±49	427±8	420±6	1.13
1232-02	0.05655±0.00077	0.53464±0.00846	0.06858±0.00095	474±31	435±6	428±6	1.61
1232-03	0.05605±0.00094	0.5264±0.00974	0.06812±0.00098	454±38	429±6	425±6	1.15
1232-04	0.05958±0.00103	0.53695±0.00992	0.06537±0.00089	588±38	436±7	440±5	1.83
1232-05	0.05771±0.00138	0.51583±0.0127	0.06486±0.00101	519±54	422±9	440±6	0.87
1232-06	0.05469±0.00076	0.5139±0.00826	0.06815±0.00094	400±32	421±6	425±6	1.11
1232-07	0.05473±0.00099	0.52473±0.01037	0.06956±0.00104	401±41	428±7	434±6	0.90
1232-08	0.05611±0.00117	0.51889±0.01133	0.06708±0.00096	457±47	424±8	419±6	0.96
1232-09	0.0566±0.00098	0.53249±0.00998	0.06824±0.00095	476±39	433±7	426±6	2.45
1232-10	0.05547±0.00107	0.5352±0.01123	0.06997±0.00109	431±44	435±7	436±7	1.11
1232-11	0.05654±0.00103	0.52696±0.01064	0.06761±0.00109	474±41	430±7	422±6	1.32

TABLE 4

(continued)

Spots	Isotopic ratios			Age/Ma (±1σ)			Th/U
	$^{207}Pb/^{206}Pb±1\sigma$	$^{207}Pb/^{235}U±1\sigma$	$^{206}Pb/^{238}U±1\sigma$	$^{207}Pb/^{206}Pb$	$^{207}Pb/^{235}U$	$^{206}Pb/^{238}U$	
Sample 1232: N27°12.035'. E112°58'820'. Hengdong Granite. 428 ± 3 Ma (n=24)							
1232-12	0.055±0.00096	0.52692±0.01027	0.06949±0.00107	412±40	430±7	433±6	0.91
1232-13	0.05502±0.00098	0.52385±0.01013	0.06906±0.00107	413±41	428±7	430±6	1.41
1232-14	0.05556±0.00156	0.522±0.01507	0.06817±0.00098	435±64	426±10	425±7	0.96
1232-15	0.05619±0.00095	0.52726±0.00988	0.06806±0.00119	460±38	430±7	424±6	0.98
1232-16	0.05885±0.00185	0.56018±0.01764	0.06904±0.00097	562±70	452±11	430±7	1.71
1232-17	0.05698±0.00097	0.54853±0.0101	0.06984±0.00113	491±38	444±7	435±6	4.53
1232-18	0.05726±0.00108	0.53623±0.01042	0.06792±0.00097	502±42	436±7	424±5	0.99
1232-19	0.05538±0.00086	0.53694±0.00936	0.07033±0.00099	428±35	436±6	438±6	0.90
1232-20	0.05545±0.00117	0.53063±0.01199	0.06942±0.00112	430±48	432±8	433±7	1.18
1232-21	0.05607±0.00104	0.53653±0.01081	0.06939±0.00103	455±42	436±7	432±6	1.50
1232-22	0.05589±0.00157	0.52872±0.01487	0.06858±0.00125	448±64	431±10	428±8	1.43
1232-23	0.05504±0.00117	0.53045±0.01194	0.06991±0.00114	414±49	432±8	436±7	1.27
1232-24	0.05484±0.00179	0.45693±0.01454	0.0604±0.00117	406±75	382±10	378±7	2.20
1232-25	0.05562±0.00105	0.53014±0.01073	0.06914±0.00105	437±43	432±7	431±6	0.82
1232-26	0.05626±0.00091	0.52981±0.00938	0.0683±0.00094	463±37	432±6	426±6	1.32
Sample 1234: N27°12.045'. E112°58'839'. Zhenzhu Granite. 427 ± 2 Ma (n=27)							
1234-01	0.05881±0.00211	0.54756±0.01915	0.06753±0.00112	560±80	443±13	421±7	0.99
1234-02	0.10339±0.00128	4.12248±0.06201	0.28922±0.00401	1686±23	1659±20	1638±20	0.85
1234-03	0.0554±0.00095	0.5413±0.01029	0.07088±0.00102	428±39	439±7	441±6	0.87
1234-04	0.05645±0.00093	0.52683±0.00988	0.0677±0.00102	470±37	430±7	422±6	1.57
1234-05	0.05627±0.00097	0.52277±0.00996	0.06739±0.00098	463±39	427±7	420±6	2.62
1234-06	0.05634±0.00115	0.53407±0.01181	0.06881±0.00113	466±46	435±8	429±7	1.45
1234-07	0.05492±0.00083	0.51777±0.00897	0.06839±0.00097	409±35	424±6	426±6	0.87
1234-08	0.05583±0.00131	0.52225±0.01285	0.06787±0.00107	446±53	427±9	423±6	1.27
1234-09	0.05556±0.00109	0.51884±0.01088	0.06774±0.00098	435±45	424±7	423±6	1.28
1234-10	0.05629±0.00141	0.52126±0.01356	0.06719±0.00111	464±57	426±9	419±7	1.55
1234-11	0.05672±0.00129	0.52498±0.01245	0.06713±0.00101	481±51	428±8	419±6	1.27
1234-12	0.05597±0.00105	0.52464±0.01082	0.068±0.00103	451±43	428±7	424±6	1.83
1234-13	0.05669±0.00124	0.52219±0.01179	0.06685±0.00095	479±49	427±8	417±6	2.45
1234-14	0.05675±0.00165	0.53099±0.01527	0.06786±0.00102	482±66	432±10	423±6	0.95
1234-15	0.0561±0.00094	0.5314±0.00984	0.06871±0.00098	456±38	433±7	428±6	1.00
1234-16	0.0563±0.00078	0.53409±0.00883	0.06882±0.00099	464±31	435±6	429±6	1.03
1234-17	0.05615±0.00134	0.53635±0.01339	0.06933±0.00116	458±54	436±9	432±7	0.82
1234-18	0.0566±0.00113	0.5337±0.01163	0.06842±0.00107	476±45	434±8	427±6	1.02
1234-19	0.05603±0.00092	0.53307±0.00987	0.06901±0.00101	454±37	434±7	430±6	1.32
1234-20	0.05519±0.00088	0.52738±0.00965	0.06931±0.00104	420±36	430±6	432±6	6.99
1234-21	0.05562±0.00091	0.53016±0.00986	0.06915±0.00103	437±37	432±7	431±6	1.49
1234-22	0.05549±0.00093	0.53232±0.00987	0.06958±0.00101	432±38	433±7	434±6	1.29
1234-23	0.05717±0.00165	0.60517±0.01735	0.07676±0.00118	498±65	481±11	477±7	1.24
1234-24	0.05601±0.00105	0.54061±0.01103	0.07001±0.00106	453±43	439±7	436±6	1.11
1234-25	0.05558±0.00146	0.52962±0.01423	0.06912±0.0011	436±60	432±9	431±7	2.39
1234-26	0.05625±0.00096	0.53315±0.01001	0.0687±0.00099	462±39	434±7	429±6	1.13
1234-28	0.05392±0.00113	0.51881±0.01159	0.06981±0.00109	368±48	424±8	435±7	1.00
1234-29	0.05479±0.00101	0.52855±0.01058	0.06997±0.00103	404±42	431±7	436±6	1.25
1234-30	0.05847±0.00188	0.54752±0.01736	0.06791±0.00106	547±72	443±11	424±6	1.32

ratios of 0.89 to 6.99. Twenty-seven analyses gave a weighted mean $^{206}Pb/^{238}U$ age of 427.4 ± 2.3 Ma (MSWD = 0.98; fig. 10D).

Furthermore, the analyses also revealed inherited zircon grains in some samples (spots 973-10,-18, 958-2,-3,-13, 1234-02), with ages of 2039 ± 20, 2441 ± 12, 2673 ± 23, 936 ± 12, 834 ± 12 Ma and 1686 ± 23 Ma (table 4), suggesting the existence of an ancient basement beneath the Wuyi and Nanling areas of the South China Fold Belt.

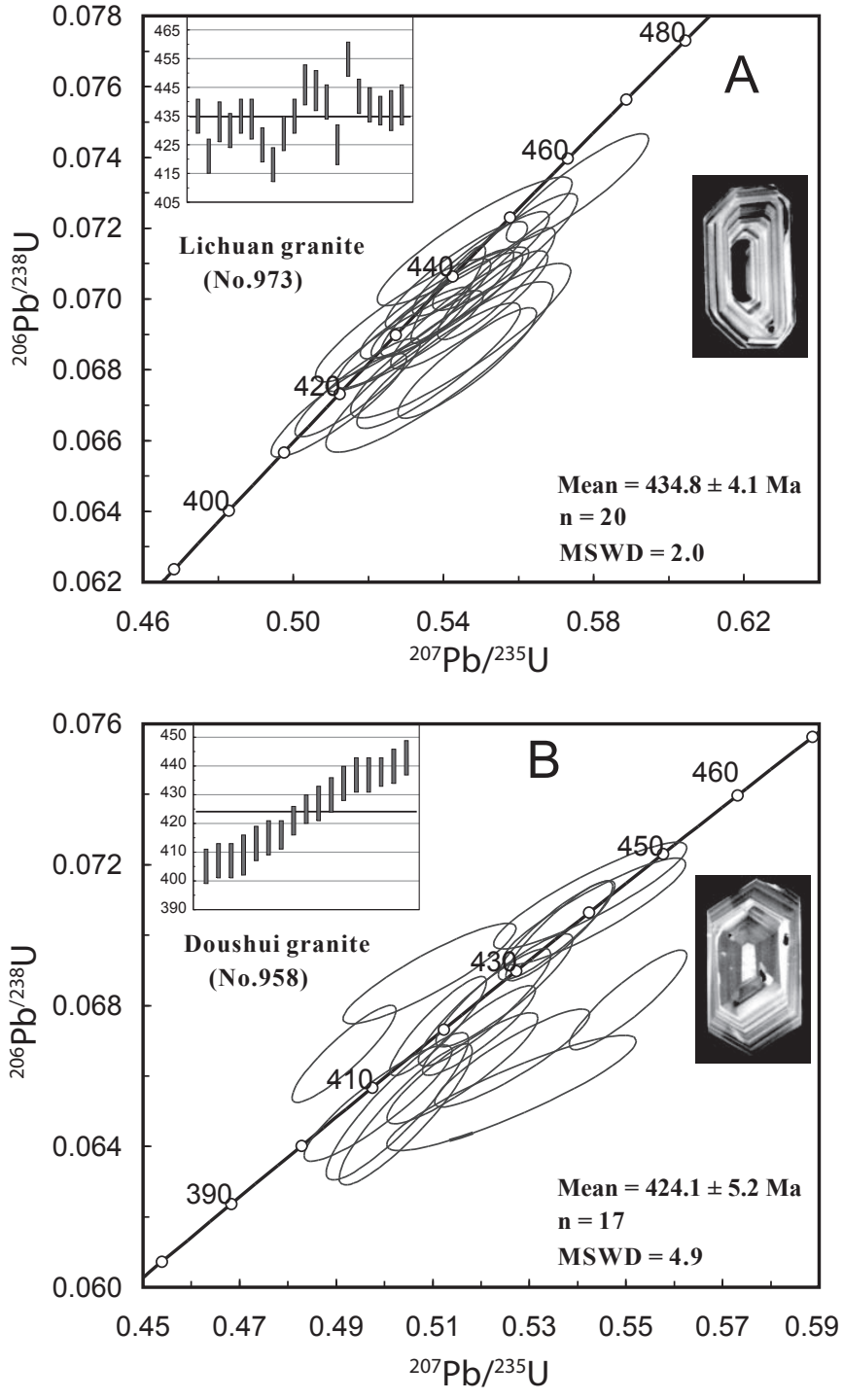

Fig. 10. Concordia $^{206}Pb/^{238}U$—$^{207}Pb/^{235}U$ diagrams of LA-ICP-MS U-Pb age data for zircons from four granitic plutons.

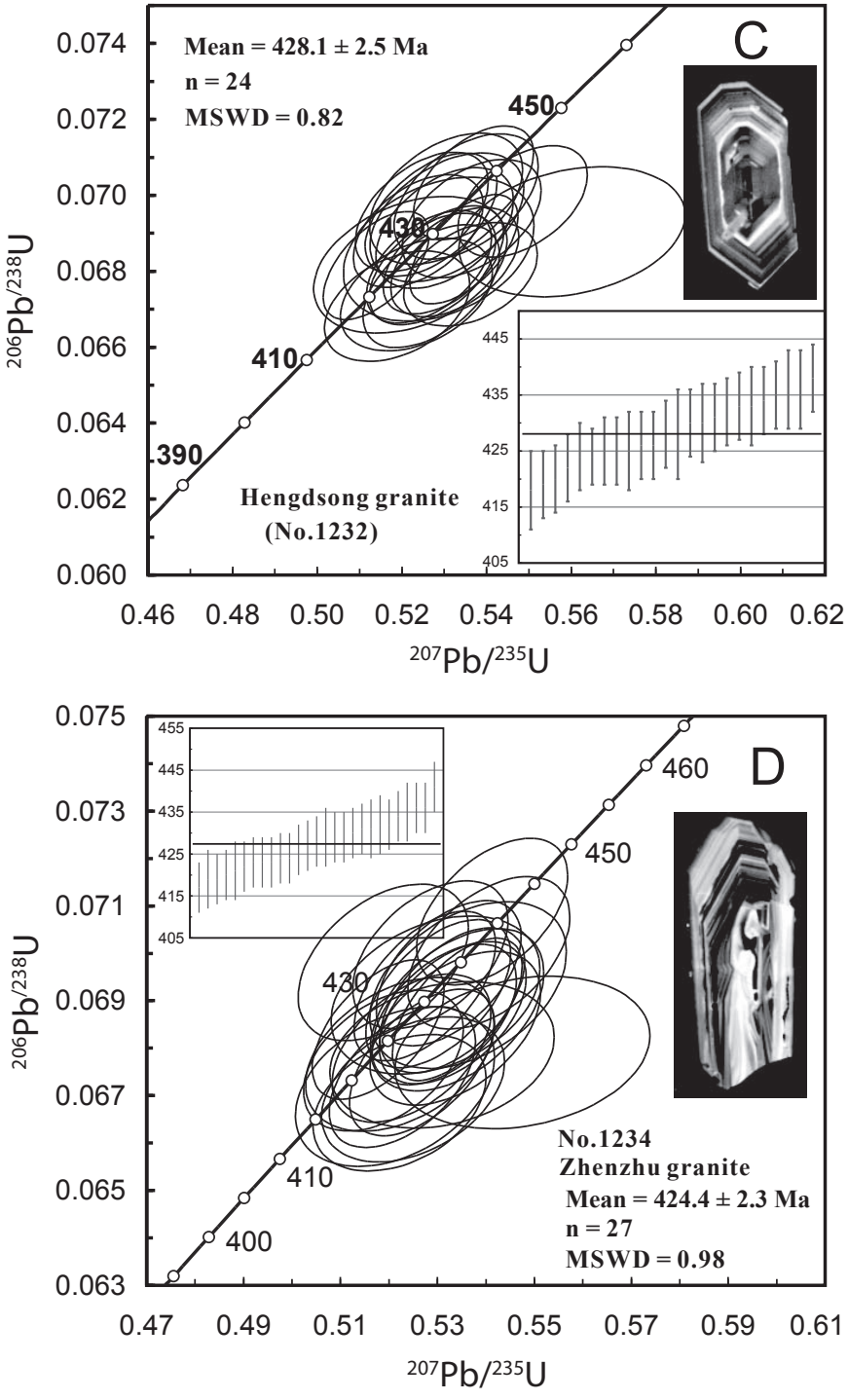

Fig. 10 (continued).

Lu–Hf isotopic compositions.—The analyzed results of Lu–Hf isotopic compositions are listed in table 5. The Lu-Hf isotopic analyses of zircons yielded negative εHf(t) values, ranging from −5.8 to −11.7 for the Doushui granite, from −7 to −12.6 for the Lichuan pluton, from −5.6 to −13.6 for the Hengdong granite, and from −4.2 to −8.5 for the Zhenzhu granitic body (table 5). The Hf isotopic data suggest that the granitic magmas were mainly derived from partial melting of crustal material, probably of Proterozoic age. This is corroborated by the two-stage Lu-Hf model ages. The ranges of two-stage model ages (T_{DM2}) are 1787 to 2241 Ma for sample 958, 1894 to 2253 Ma for sample 973, 1769 to 1953 Ma for sample 1232, and 1666 to 1933 Ma for sample 1234. A model for the generation of the granitic magmas by partial melting of the Paleoproterozoic basement is illustrated in figure 11. The involvement of the mantle component is arguably absent (Xiang and Shu, 2010; Yao and others, 2011; Y. Zhang and others, 2011).

DISCUSSION AND CONCLUSION

Depositional Environment of South China in the Early Paleozoic

As described above, distinct early Paleozoic stratigraphic sequences occur in the Jiangnan, and Cathaysian domains and the intervening zone (fig. 2). In the Jiangnan, the 1520 m thick Cambrian sequence represents pyrite-phosphate-bearing mudstone, limestone and marlite, containing abundant *Trilobite* and *Brachiopoda*; the 920 m thick Ordovician strata consist of bioclastic limestone, nodular marlite and sandstone, in which abundant *Brachiopoda, Coral, Graptolite* and *Cephalopoda* are well preserved; the 2870 m thick Silurian succession shows a lithologic association of siltstone and mudstone, containing *Brachiopoda* and some *Graptolite*. The strata of three successions witnessed a neritic depositional environment.

In contrast, a *Graptolite-bearing* clastic succession was widely accumulated in the Cathaysia block during the early Paleozoic (GXBGMR, 1984; JXBGMR, 1984; HNBGMR, 1987; ZJBGMR, 1989) (fig. 12). Along a N-S direction, a southward thickening trend in the period from early Cambrian to middle Ordovician can be distinguished from figure 2. During late Ordovician, an olistostrome depositional sequence (O_3h+O_3s=920 m) occurred in the northern Cathaysia block (fig. 2B) whereas the coeval sandy-muddy assemblage of 2050 m thick was developed in the zone linking between Jiangnan and Cathaysia (fig. 2C).

To the southwestern extension of the study area, the Paleozoic depositional sequences show different composition and thickness. The muddy component gradually increased and carbonate component was decreased (fig. 12), suggesting that the basin became deeper toward the Hunan, Guangxi and Yunnan areas (GXBGMR, 1984; HNBGMR, 1987; YNBGMR, 1988). In southeast Guangxi Province, a very thick (>10,000 m) early Paleozoic sequence is preserved, and the littoral sedimentary structures, such as ripple mark, gradually decrease and even disappear toward the southwest (fig. 12). These changes indicate that the water depth increased toward the southwest during the early Paleozoic.

Provenance of the Early Paleozoic Clastic Rocks

The early Paleozoic clastic rocks in the study area were previously considered to be derived from both the Proterozoic mantle-derived volcanic rocks and the sedimentary rocks of the Yangtze block (B. J. Liu and others, 1993; Wu, 2005). Field observation suggests that the paleo-current directions between the eastern and western segments of Cathaysia are rather consistent, being NW- and W-oriented. This supports the proposal of Ren and others (1990) that the early Paleozoic sediments were mostly derived from the southeastern and eastern parts of Cathaysia. In fact, basement rocks of Paleoproterozoic ages (1.73 Ga) have been confirmed in the South China Sea and the East

Table 5

The Hf isotope compositions for in situ zircons from four granites in the South China Fold Belt

Samples	$^{176}Yb/^{177}Hf$	$^{176}Lu/^{177}Hf$	2σ	$^{176}Hf/^{177}Hf$	2σ	εHf(0)	εHf(t)	2σ	T_{DM1}(Ma)	T_{DM2}(Ma)	$f_{Lu/Hf}$
Sample 973: GPS N27°11.118', E116°43'206', Lichuan Granite, 434.8 ± 4.1 Ma (n=20)											
973-1	0.024124	0.00100222	0.000002	0.282069287	0.000011	-24.85	-10.08	0.43	1667	2250	-0.97
973-2	0.010972	0.00044426	0.000002	0.282242592	0.000016	-18.72	-8.59	0.57	1403	1981	-0.99
973-3	0.020387	0.00076823	0.000006	0.28221938	0.000017	-19.54	-9.71	0.60	1447	2045	-0.98
973-4	0.011322	0.00042773	0.000002	0.28221216	0.000012	-19.80	-9.86	0.43	1444	2054	-0.99
973-5	0.015423	0.00058858	0.000003	0.28219874	0.000015	-20.27	-10.34	0.52	1469	2086	-0.98
973-6	0.014741	0.00056307	0.000002	0.282285332	0.000012	-17.21	-7.86	0.42	1350	1916	-0.98
973-7	0.018284	0.000685	0.000003	0.282286	0.000015	-17.18	-7.30	0.51	1351	1894	-0.98
973-8	0.018911	0.00082468	0.000002	0.282074306	0.000007	-24.67	-10.49	0.34	1652	2253	-0.98
973-9	0.019901	0.00077776	0.000005	0.28222568	0.000014	-19.32	-9.52	0.49	1439	2031	-0.98
973-11	0.017202	0.00062476	0.000002	0.28226222	0.000017	-18.03	-8.13	0.59	1383	1946	-0.98
973-12	0.023262	0.00086984	0.000004	0.28223797	0.000017	-18.89	-9.07	0.61	1425	2005	-0.97
973-13	0.001178	0.00032243	0.000001	0.282145653	0.000009	-22.15	-12.61	0.32	1522	2217	-1.00
973-14	0.015865	0.000586	0.000002	0.282251	0.000013	-18.42	-8.51	0.48	1396	1970	-0.98
973-15	0.010170	0.00037874	0.000001	0.282244069	0.000013	-18.67	-8.65	0.47	1399	1980	-0.99
973-16	0.012917	0.00048842	0.000000	0.282282000	0.000013	-17.33	-7.43	0.46	1350	1900	-0.99
973-17	0.015623	0.00058586	0.000004	0.282271111	0.000014	-17.71	-7.36	0.50	1369	1914	-0.98
973-19	0.021301	0.00080408	0.000002	0.282246645	0.000013	-18.58	-6.97	0.44	1411	1937	-0.98
973-20	0.022445	0.00081750	0.000005	0.28223758	0.000015	-18.90	-9.09	0.52	1424	2005	-0.98
973-21	0.030537	0.00110622	0.000002	0.282071032	0.000008	-24.79	-9.59	0.32	1669	2236	-0.97
973-22	0.013196	0.00049324	0.000002	0.282239848	0.000012	-18.82	-8.88	0.42	1409	1993	-0.99
Sample 958: N25º49.440', E114º24.817', Doushui Granite, 424.1 ± 5.2 Ma (n=17)											
958-1	0.015693	0.00060153	0.000002	0.282343449	0.000017	-15.16	-5.84	0.57	1271	1787	-0.98
958-4	0.013196	0.000493	0.000002	0.282240	0.000012	-18.82	-8.88	0.42	1409	1993	-0.99
958-5	0.008266	0.00028700	0.000002	0.282105234	0.000015	-23.58	-11.66	0.44	1587	2241	-0.99
958-6	0.019402	0.00076970	0.000005	0.282324046	0.000017	-15.84	-6.01	0.59	1302	1812	-0.98
958-7	0.012091	0.00046867	0.000001	0.282254851	0.000018	-18.29	-8.82	0.57	1389	1980	-0.99
958-8	0.014762	0.00055776	0.000003	0.282237504	0.000013	-18.90	-8.87	0.47	1414	1997	-0.98
958-9	0.023262	0.000870	0.000004	0.282238	0.000017	-18.89	-9.07	0.61	1425	2005	-0.97
958-10	0.012147	0.00042770	0.000002	0.28226161	0.00001	-18.05	-8.79	0.42	1378	1970	-0.99
958-11	0.019661	0.00072022	0.000004	0.282311579	0.000013	-16.28	-6.91	0.53	1319	1858	-0.98
958-12	0.023304	0.000882	0.000005	0.282275	0.000019	-17.58	-7.69	0.68	1374	1921	-0.97

Table 5
(continued)

Samples	$^{176}Yb/^{177}Hf$	$^{176}Lu/^{177}Hf$	2σ	$^{176}Hf/^{177}Hf$	2σ	εHf(0)	εHf(t)	2σ	T_{DM1}(Ma)	T_{DM2} (Ma)	$f_{Lu/Hf}$
Sample 958: N25º49.440', E114º24.817', Doushui Granite, 424.1 ± 5.2 Ma (n=17)											
958-14	0.012200	0.000464	0.000003	0.282222	0.000013	-19.46	-8.98	0.47	1432	2019	-0.99
958-15	0.015512	0.00057476	0.000002	0.282283367	0.000012	-17.28	-7.30	0.44	1352	1896	-0.98
958-16	0.006832	0.00024400	0.000002	0.282239000	0.000017	-18.85	-7.15	0.45	1402	1949	-0.99
958-17	0.018284	0.00068506	0.000003	0.282286278	0.000015	-17.18	-7.30	0.51	1351	1894	-0.98
958-18	0.011724	0.000439	0.000002	0.282252	0.000011	-18.40	-8.34	0.37	1391	1963	-0.99
958-19	0.012104	0.000454	0.000002	0.282223	0.000016	-19.42	-9.42	0.55	1430	2029	-0.99
958-20	0.0104517	0.00036543	0.000004	0.282288698	0.000011	-17.09	-7.55	0.42	1338	1901	-0.99
Sample 1232: N27°12.035', E112°58'820', Hengdong Granite, 428 ± 3 Ma (n=24)											
1232-01	0.016824	0.000735	0.000015	0.282388	0.000022	-13.57	-13.57	0.63	1213	1953	-0.98
1232-02	0.027727	0.001160	0.000024	0.282300	0.000027	-16.67	-7.77	0.41	1350	1900	-0.97
1232-03	0.021334	0.000909	0.000016	0.282349	0.000025	-14.97	-5.82	0.52	1274	1783	-0.97
1232-04	0.027843	0.001133	0.000015	0.282284	0.000026	-17.24	-8.23	0.57	1372	1933	-0.97
1232-05	0.008477	0.000371	0.000002	0.282271	0.000019	-17.70	-8.84	0.57	1362	1959	-0.99
1232-06	0.017488	0.000716	0.000008	0.282344	0.000024	-15.14	-6.44	0.45	1274	1805	-0.98
1232-07	0.015416	0.000660	0.000021	0.282354	0.000020	-14.79	-5.64	0.48	1258	1769	-0.98
1232-08	0.023436	0.000967	0.000019	0.282344	0.000020	-15.13	-5.87	0.32	1282	1791	-0.97
1232-09	0.062360	0.002427	0.000015	0.282356	0.000025	-14.69	-6.16	0.68	1316	1798	-0.93
1232-10	0.015865	0.000676	0.000005	0.282292	0.000018	-16.96	-7.80	0.62	1344	1907	-0.98
1232-11	0.011273	0.000489	0.000022	0.282353	0.000020	-14.83	-5.39	0.45	1254	1762	-0.99
1232-12	0.014959	0.000614	0.000004	0.282315	0.000022	-16.14	-7.05	0.42	1310	1856	-0.98
1232-13	0.016725	0.000692	0.000039	0.282337	0.000021	-15.37	-6.05	0.47	1282	1802	-0.98
1232-14	0.024880	0.001014	0.000036	0.282316	0.000020	-16.13	-6.97	0.52	1323	1857	-0.97
1232-15	0.015729	0.000686	0.000004	0.282302	0.000018	-16.64	-7.50	0.39	1332	1887	-0.98
1232-16	0.022039	0.000905	0.000036	0.282310	0.000020	-16.34	-7.28	0.51	1328	1873	-0.97
1232-17	0.016742	0.000735	0.000016	0.282335	0.000020	-15.47	-6.23	0.41	1288	1811	-0.98
1232-18	0.018754	0.000816	0.000012	0.282306	0.000017	-16.49	-7.17	0.58	1331	1874	-0.98
1232-19	0.014861	0.000615	0.000021	0.282300	0.000020	-16.70	-7.56	0.45	1332	1890	-0.98
1232-20	0.013563	0.000587	0.000007	0.282277	0.000016	-17.49	-8.04	0.45	1362	1931	-0.98
1232-21	0.019031	0.000826	0.000042	0.282282	0.000019	-17.34	-8.06	0.43	1364	1929	-0.98
1232-22	0.018250	0.000798	0.000018	0.282352	0.000017	-14.85	-5.58	0.56	1265	1771	-0.98

Table 5

(continued)

Samples	$^{176}Yb/^{177}Hf$	$^{176}Lu/^{177}Hf$	2σ	$^{176}Hf/^{177}Hf$	2σ	εHf(0)	εHf(t)	2σ	T_{DM1}(Ma)	T_{DM2} (Ma)	$f_{Lu/Hf}$
Sample 1234: N27°12.045', E112°58'839', Zhenzhu Granite, 427 ± 2 Ma (n=27)											
1234-01	0.018990	0.000770	0.000006	0.282364	0.000027	-14.42	-5.88	0.37	1248	1765	-0.98
1234-02	0.054460	0.002085	0.000048	0.282346	0.000025	-15.07	-6.96	0.42	1319	1829	-0.94
1234-03	0.028666	0.001106	0.000040	0.282343	0.000026	-15.16	-6.80	0.56	1288	1819	-0.97
1234-04	0.017541	0.000720	0.000006	0.282346	0.000020	-15.08	-6.44	0.58	1272	1803	-0.98
1234-05	0.016295	0.000631	0.000007	0.282385	0.000026	-13.67	-4.83	0.47	1213	1707	-0.98
1234-06	0.052404	0.001959	0.000038	0.282383	0.000027	-13.75	-5.40	0.38	1261	1738	-0.94
1234-07	0.028144	0.001140	0.000024	0.282409	0.000024	-12.85	-4.22	0.36	1197	1666	-0.97
1234-08	0.013230	0.000525	0.000007	0.282351	0.000023	-14.89	-5.83	0.31	1258	1777	-0.98
1234-09	0.030335	0.001185	0.000016	0.282291	0.000029	-17.02	-8.49	0.63	1365	1933	-0.96
1234-10	0.026955	0.001072	0.000004	0.282319	0.000025	-16.03	-7.57	0.57	1321	1871	-0.97
1234-11	0.024207	0.000957	0.000010	0.282342	0.000021	-15.19	-6.68	0.43	1284	1816	-0.97
1234-12	0.023892	0.000958	0.000024	0.282362	0.000022	-14.49	-5.83	0.41	1256	1767	-0.97
1234-13	0.036491	0.001374	0.000027	0.282374	0.000022	-14.08	-5.42	0.43	1254	1745	-0.96
1234-14	0.025062	0.000997	0.000019	0.282333	0.000023	-15.52	-6.59	0.42	1298	1825	-0.97
1234-15	0.039085	0.001523	0.000039	0.282361	0.000024	-14.52	-5.59	0.38	1277	1767	-0.95
1234-16	0.028311	0.001135	0.000049	0.282389	0.000025	-13.55	-4.64	0.47	1225	1702	-0.97
1234-17	0.060107	0.002230	0.000017	0.282377	0.000023	-13.97	-5.55	0.45	1279	1753	-0.93
1234-18	0.073455	0.002718	0.000088	0.282383	0.000025	-13.75	-5.56	0.57	1287	1750	-0.92
1234-19	0.028310	0.001118	0.000024	0.282361	0.000019	-14.55	-6.29	0.43	1264	1784	-0.97
1234-20	0.022992	0.000908	0.000008	0.282359	0.000021	-14.62	-5.92	0.38	1260	1774	-0.97
1234-21	0.024463	0.000970	0.000010	0.282368	0.000020	-14.27	-5.61	0.41	1248	1753	-0.97
1234-22	0.021441	0.000838	0.000019	0.282345	0.000023	-15.09	-6.14	0.53	1276	1796	-0.97

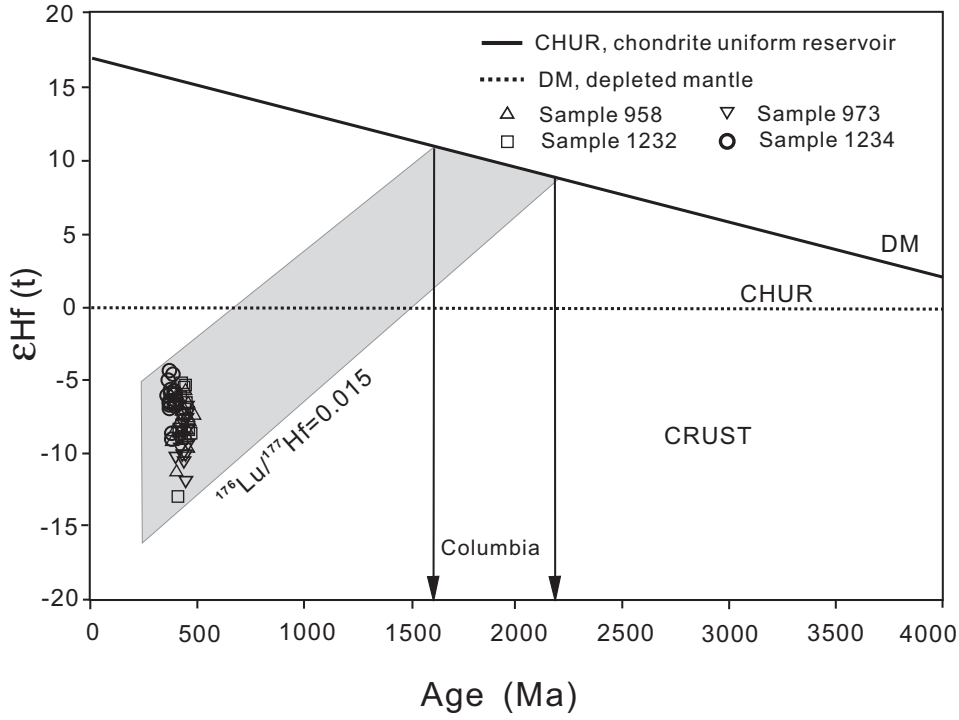

Fig. 11. Epsilon Hf vs. U–Pb age for the zircons.

China Sea (Ren and others, 1990, 1998; Sun and others, 2013). Mantle xenoliths from the Penghu Island (Taiwan Strait) also reveal the presence of Proterozoic lithospheric mantle (K. L. Wang and others, 2003).

The northwestern side of the study area belongs to the Jiangnan belt, in which the early Paleozoic rock assemblages are characterized by carbonate and chert. The absence of SE-ward paleocurrents makes it unlikely that the Jiangnan belt provided significant amount of clastic sediments to Cathaysia during the early Paleozoic. In other words, the principal source of the early Paleozoic sediments is most likely located to the southeast-east of the study area. Ren (1964) and Ren and others (1990) called this hypothesized provenance as "the split South China Sea Oldland" which was later submerged or buried.

The Nd two-stage model ages derived from the pre-Devonian clastic rocks in Cathaysia are mostly older than 2.0 Ga (2.26-2.47 Ga), whereas the coeval clastic rocks from the Jiangnan domain yielded younger model ages, a model age range of 1.82 to 1.90 Ga (Shen and others, 2009).

Correspondingly, the Cambrian-Ordovician sedimentary rocks in Cathaysia have negative $\varepsilon_{Nd}(t)$ values of −12.8 to −15.2, and the coeval clastic rocks from the Jiangnan show higher $\varepsilon_{Nd}(t)$ values of −9.7 to −11.6 (Shen and others, 2009). More than 90 percent of the detrital zircons from Cathaysia show negative εHf(t) values (−9.2 to −13.2) (Yao and others, 2012), suggesting that their source was dominated by recycling of old upper continental crustal material. The contribution of the mantle component (depleted mantle-derived rocks) to the Paleozoic sedimentary rocks should not be significant for most of the regions.

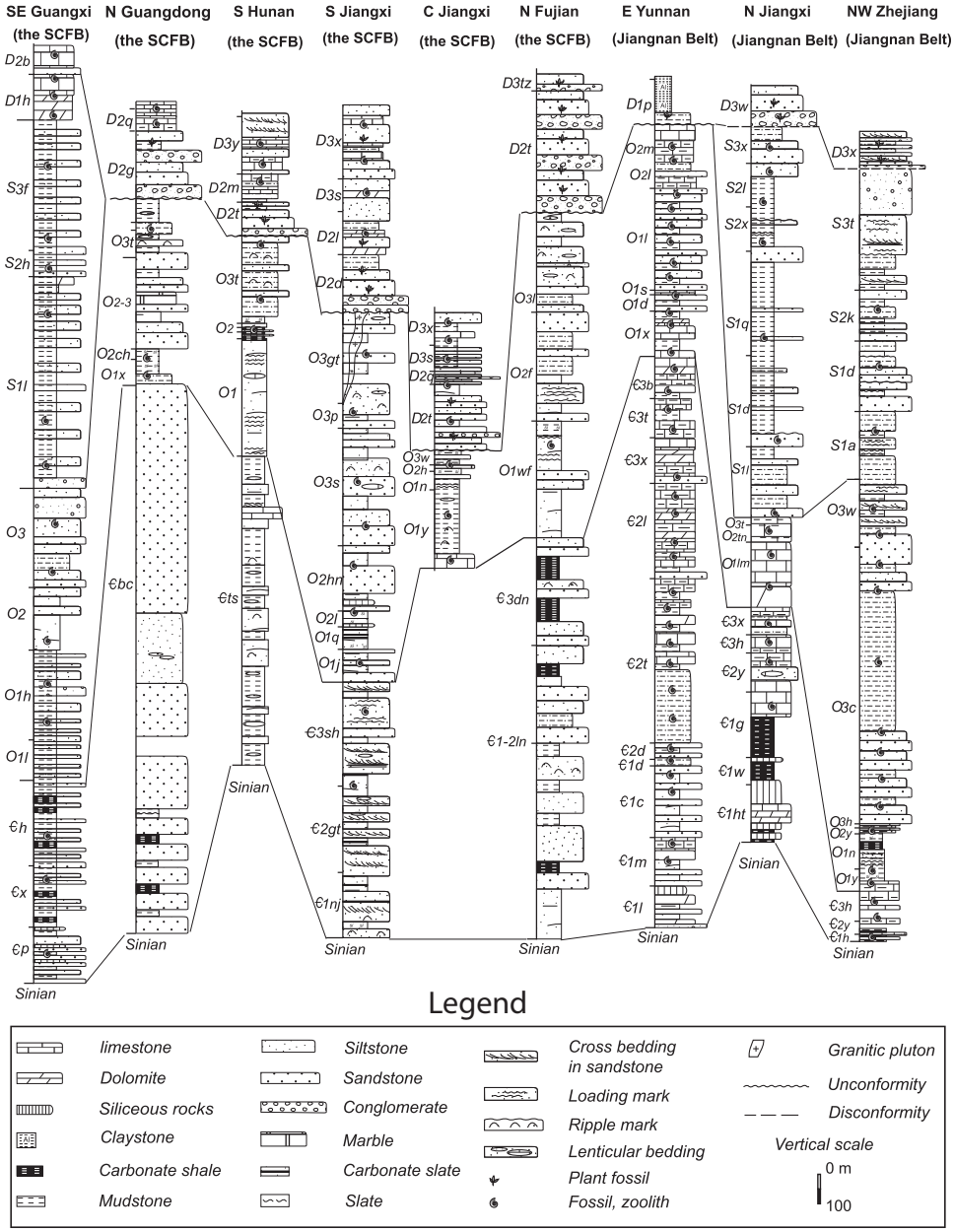

Fig. 12. Comparison of the early Paleozoic depositional sequences in the different segments of South China.

Finally, based on the published detrital zircon ages of >400 Ma, five major age populations can be recognized: 2560 to 2380 Ma (a peak of 2460 Ma), 1930 to 1520 Ma (a peak of 1700 Ma), 1300 to 900 Ma (a major peak at 970 Ma), 850 to 730 Ma (a prominent peak of 780 Ma) and 670 to 530 Ma (a major peak at 540 Ma) (X. S. Xu and others, 2005; Yu and others, 2007; Xiang and Shu, 2010). These populations corre-

spond to five major global tectonothermal events (Yao and others, 2011, 2012; Shu and others, 2011b). The Hf model age data suggest that the major crustal growth in Cathaysia took place at 1.6 to 2.8 Ga; a large proportion (30-40%) of zircon grains are euhedral to sub-euhedral, implying that they were derived from a proximal source.

Geodynamics of the Early Paleozoic South China Fold Belt

During the late Neoproterozoic, following the completion of the Jiangnan orogeny (Guo and others, 1989; Shu and Charvet, 1996), lithospheric-scale extension occurred in South China. This event corresponds to a global-scale supercontinent breakup (Z. X. Li and others, 2003). The extension led to a strong thinning of the crust that is characterized by rift basins filled with coarse clastic rocks and bimodal volcanic rocks dated at 810 to 790 Ma (J. Wang and Li, 2003). The South China Craton was rifted along the Shaoxing-Jiangshan-Pingxiang fault zone (Shu, 2006) and the Cathaysia block was further split into three sub-blocks, namely, Wuyi, Nanling and Yunkai (Shu and others, 2011a). The extensional zone between Yangtze and Cathaysia and the zones between the sub-blocks evolved into rift basins containing interbanded rhyolite and alkaline basalt and subsequently into marine basins filled with a thick Sinian and early Paleozoic siliciclastic sediments (G. W. Zhang and others, 2013). The tectonic framework was similar to an archipelagic sea (compare, Yin and others, 1999).

In the late Ordovician, a regional compression was accommodated by the northwest-ward underthrusting of a block that possibly occupied a position corresponding to the current position of the South China and East China seas beneath the southeastern Cathaysia, whereas a southeast-ward underthrusting of the Jiangnan domain beneath the northwestern Cathaysia block (fig. 13A). This event was accompanied by anatexis and emplacement of S-type granitoids dated at 440 to 400 Ma. Southeast Cathaysia witnessed a southeastward intra-crustal ductile thrusting whereas northwest Cathaysia experienced northwestward intra-crustal ductile thrusting with Ar-Ar ages of 430 to 390 Ma (Shu and others, 1999; Charvet and others, 2010; X. B. Xu and others, 2011), resulting in a fan-shape thrusting pattern (fig. 13B). During this geodynamic process, there was no mantle-derived magmatic activity.

Early Paleozoic orogenesis led to the re-amalgamation of various blocks, forming the South China Fold Belt and the united South China continent. The thick middle Devonian conglomerate and quartz-sandstone sequence (500-2000 m thick) and the regional-scale angular unconformity provide further evidence for the early Paleozoic orogeny.

In contrast with the typical collisional orogenic belts of the world, the early Paleozoic South China Fold Belt developed on the Cathaysia basement shows some distinct features: (1) absence of early Paleozoic ophiolite and volcanic rocks, (2) lack of syntectonic high-pressure metamorphic rocks despite the strong folding, ductile shearing, HT metamorphism and migmatization, (3) scarcity of mantle-derived rocks of early Paleozoic age, (4) absence of a typical turbidite with Bouma sequence, and (5) Hf isotopic data suggesting that the Silurian granites were mainly derived from partial melting of Paleoproterozoic crust material with little or no input of mantle-derived rocks. We therefore consider that the early Paleozoic South China Fold Belt is not a subduction-collision-type orogen but an intraplate orogen that developed in response to the global supercontinent assembly of Gondwana. The major geodynamic process involved the initial formation of a failed rift (aulacogen) and its closure by underthrusting of intra-plate blocks (fig. 13). With ophiolites, arc magmatism and HP metamorphic rocks conspicuously absent, this orogen shows similarities with intraplate orogens, such as the Cenozoic Tianshan in Central Asia and the European Pyrenean Chain (Roure and others, 1989; Choukroune and others, 1990; Garcia-Senz and others, 2000; Debelmas and Mascle, 2004; Charvet and others, 2010).

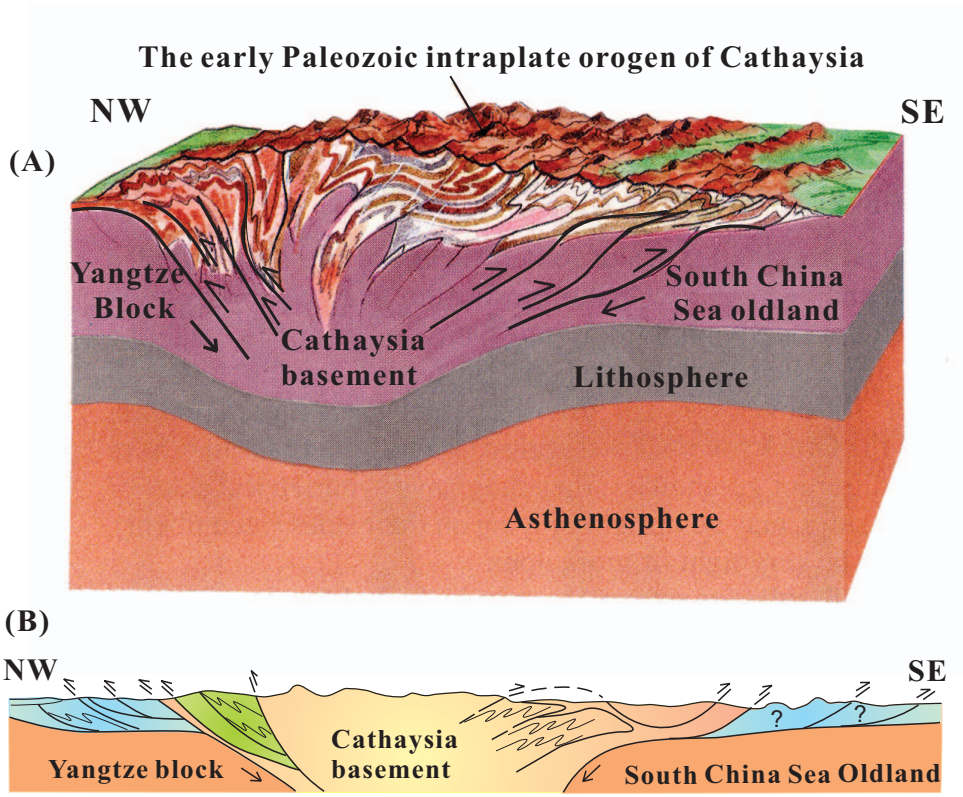

Fig. 13. Schematic model (A) of the early Paleozoic intraplate orogeny in Cathaysia, showing a fan-shape thrusting pattern (B).

CONCLUDING REMARKS

1. The early Paleozoic sedimentary sequences in the study area were formed in a neritic-bathyal or slope depositional environment, whereas the late Ordovician was a transitional period from neritic-bathyal into littoral-land environment. Paleo-current measurements indicate a northwestward and westward transport, suggesting that the provenances were located to the eastern and southeastern sides of Cathaysia.

2. Geochemical data from early Paleozoic clastic rocks suggest that the Cambrian sandstones were sourced from stable provenance whereas the Ordovician clastic rocks were derived from multiple sources. The sedimentary rocks show negative $\varepsilon_{Nd}(t)$ values (-7.9 to -13.9) and Paleoproterozoic two-stage model ages (2.04-2.36 Ga), suggesting that these sedimentary rocks were derived from Paleoproterozoic rocks.

3. During the Silurian, regional-scale folding, thrusting and large-scale anatexis occurred in Cathaysia. Kinematic indicators from coeval ductile sheared rocks show a fan-shape thrusting pattern. ^{40}Ar-^{39}Ar dating on neo-formed micas yielded ages of 430 to 390 Ma, which are broadly similar to zircon U-Pb ages (440-400 Ma) of the syntectonic granitoids.

4. Zircon U-Pb dating of four granitic plutons yielded a range of $^{206}Pb/^{238}U$ ages from 425 Ma to 435 Ma. All the zircon εHf(t) values are negative and show a peak of Hf two-stage model ages around 1.9 Ga, indicating that the Silurian granitic magma was derived from the recycling of Paleoproterozoic basement.

5. In contrast with typical collisional belts of the world, the early Paleozoic South China Fold Belt shows some distinct features: absence of coeval ophiolite and volcanic rocks, lack of HP-type metamorphic rocks and no mantle-derived magmatic rocks. We therefore do not favour the model of South China Fold Belt as a typical subduction-collision-type orogenic belt. Instead, we consider it as an intraplate orogen developed through the closure of rift basins, and correlate the geodynamics with the early Paleozoic global assembly of Gondwana.

ACKNOWLEDGMENTS

We thank Peter Cawood and Min Sun for their constructive reviews and comments. We are particularly grateful to P. Cawood for his extensive corrections and suggestions on the text, which led to major improvements of the manuscript. We acknowledge the financial supports provided by the National Basic Research Program of China (973 Program, No. 2012CB416701), National Natural Science Foundation of China (No. 41272226), the Ministry of Land and Resources (No. 201211093-1) and the Education Ministry of China (No.20120091110024). Bor-ming Jahn acknowledges the support of National Research Council (Taiwan) through grants NSC-100-2116-M-002-024 and NSC-101-2116-M-002-003. This study also contributes to the 1000 Talent Award to M. Santosh from Chinese Government.

References

Bhatia, M. R., 1983, Plate tectonics setting of sandstones and geochemical composition of sandstones: Journal of Geology, v. 91, n. 6, p. 611–627, http://dx.doi.org/10.1086/628815

——— 1985, Rare earth element geochemistry of Australian Paleozoic greywackes and mudrocks: Provenance and tectonic control: Sedimentary Geology, v. 45, n. 1–2, p. 97–113, http://dx.doi.org/10.1016/0037-0738(85)90025-9

Bhatia, M. R., and Crook, K. A. W., 1986, Trace element characteristics of graywackes and tectonic setting discrimination of sedimentary basins: Contributions to Mineralogy and Petrology, v. 92, n. 2, p. 181–193, http://dx.doi.org/10.1007/BF00375292

Bhatia, M. R., and Taylor, S. R., 1981, Trace-element geochemistry and sedimentary provinces: A study from the Tasman geosyncline, Australia: Chemical Geology, v. 33, n. 1–4, p. 115–125, http://dx.doi.org/10.1016/0009-2541(81)90089-9

Black, L. P., Kamo, S. L., Williams, I. S., Mundil, R., Davis, D. W., Korsch, R. J., and Foudoulis, C., 2003, The application of SHRIMP to Phanerozoic geochronology; a critical appraisal of four zircon standards: Chemical Geology, v. 200, n. 1–2, p. 171–188, http://dx.doi.org/10.1016/S0009-2541(03)00166-9

Charvet, J., Shu, L., Faure, M., Choulet, F., Wang, B., Lu, H., and Le Breton, N., 2010, Structural development of the Lower Paleozoic belt of South China: Genesis of an intracontinental orogen: Journal of Asian Earth Sciences, v. 39, n. 4, p. 309–330, http://dx.doi.org/10.1016/j.jseaes.2010.03.006

Chen, J., Foland, K. A., Xing, F., Xu, X., and Zhou, T., 1991, Magmatism along the southeast margin of the Yangtze block: Precambrian collision of the Yangtze and Cathaysia blocks of China: Geology, v. 19, n. 8, p. 815–818, http://dx.doi.org/10.1130/0091-7613(1991)019⟨0815:MATSMO⟩2.3.CO;2

Chen, X., Zhang, Y. D., Fan, J. X., Cheng, J. F., and Li, Q. J., 2010, Ordovician graptolite-bearing strata in southern Jiangxi with a special reference to the Kwangsian Orogeny: Science China: Earth Sciences, v. 53, n. 11, p. 1602–1610, http://dx.doi.org/10.1007/s11430-010-4117-6

Chen, X., Zhang, Y. D., Fan, J. X., Tang, L., and Sun, H. Q., 2012, Onset of the Kwangsian Orogeny as evidenced by biofacies and lithofacies: Science China: Earth Sciences, v. 55, n. 10, p. 1592–1600, http://dx.doi.org/10.1007/s11430-012-4490-4

Choukroune, P., Roure, F., and Pinet, B., 1990, Main results of the ECORS Pyrenees profile:Tectonophysics, v. 173, n. 1–4, p. 411–423, http://dx.doi.org/10.1016/0040-1951(90)90234-Y

Compston, W., Williams, I. S., Kirchvink, J. L., Zichao, S., and Guogan, M. A., 1992, Zircon U-Pb ages for the Early Cambrian time scale: Journal of the Geological Society, London, v. 149, n. 2, p. 171–184, http://dx.doi.org/10.1144/gsjgs.149.2.0171

Debelmas, J., and Mascle, G., 2004, Les grandes structures geologiques: Paris, Masson, Paperback, p. VIII +299.

Faure, M., Shu, L., Wang, B., Charvet, J., Choulet, F., and Monié, P., 2009, Intracontinental subduction: a possible mechanism for the Early Palaeozoic Orogen of SE China: Terre Nova, v. 21, n. 5, p. 360–368, http://dx.doi.org/10.1111/j.1365-3121.2009.00888.X

FJBGMR (Fujian Bureau of Geology and mineral Resources), 1985, Regional Geology of Fujian Province: Beijing, Geological Publishing House, 617 p. (in Chinese with English abstract).

Garcia-Senz, J., Munoz, J. A., and McClay, K., 2000, Inversion of Early Cretaceous extensional basins in the central Spanish Pyrenees: Bali, Indonesia, AAPG International Conference and Meeting, Poster and extended abstracts (Published in CD-ROM) AAPG Bulletin, v. 84, n. 9, p. 1428–1429.

GDBGMR (Guangdong Bureau of Geology and Mineral Resources), 1988, Regional geology of Guangdong Province: Beijing, Geological Publishing House, 941 p. (in Chinese with English abstract).
Gilder, S. A., Keller, G. R., Luo, M., and Godell, P. G., 1991, Eastern Asia and the western Pacific timing and spatial distribution of rifting in China: Tectonophysics, v. 197, n. 2–4, p. 225–243, http://dx.doi.org/10.1016/0040-1951(91)90043-R
Grabau, A. W., 1924, Stratigraphy of China, Part I, Paleozoic and older: Peking, The Geological Survey of Agriculture and Commerce, v. 528, p. 1–6.
Griffin, W. L., Wang, X., Jackson, S. E., Pearson, N. J., O'Reilly, S. Y., Xu, X., and Zhou, X., 2002, Zircon chemistry and magma mixing, SE China: In-situ analysis of Hf isotopes, Tonglu and Pingtan igneous complexes: Lithos, v. 61, n. 3–4, p. 237–269, http://dx.doi.org/10.1016/S0024-4937(02)00082-8
Guo, L., Shi Y., Lu, H., Ma, R., Dong, H., and Yang, S., 1989, The pre-Devonian tectonic patterns and evolution of South China: Journal of Southeast Asian Earth Sciences, v. 3, n. 1–4, p. 87–93, http://dx.doi.org/10.1016/0743-9547(89)90012-3
GXBGMR (Guangxi Bureau of Geology and Mineral Resources), 1984, Regional geology of Guangxi Zhuang Autonomous Region: Beijing, Geological Publishing House, 853 p. (in Chinese with English abstract).
HNBGMR (Hunan Bureau of Geology and Mineral Resources), 1987, Regional Geology of Hunan Province: Beijing, Geological Publishing House, 650 p. (in Chinese with English abstract).
Hsü, K. J., Sun, S., Li, J., Chen, H., Peng, H., and Sengör, A. M. C., 1988, Mesozoic overthrust tectonics in South China: Geology, v. 16, n. 5, p. 418–421, http://dx.doi.org/10.1130/0091-7613(1988)016(0418:MOTISC)2.3.CO;2
Hu, G. R., and Zhang, B. D., 1998, The Nd isotopic compositions and their source areas of the metamorphic basement of Central Jiangxi Province: Acta Petrologica et Mineralogica, v. 17, n. 1, p. 35–39 (in Chinese with English abstract).
Jackson, S. E., Pearson, N. J., Griffin, W. L., and Belousova, E. A., 2004, The application of laser ablation microprobe-inductively coupled plasma-mass spectrometry to in situ U-Pb zircon geochronology: Chemical Geology, v. 211, n. 1–2, p. 47–69, http://dx.doi.org/10.1016/j.chemgeo.2004.06.017
Jahn, B.-M., 1974, Mesozoic thermal events in southeast China: Nature, v. 248, p. 480–483, http://dx.doi.org/10.1038/248480a0.
——— 2010, Accretionary orogen and evolution of the Japanese Islands: Implications from a Sr-Nd isotopic study of the Phanerozoic granitoids from SW Japan: American Journal of Science, v. 310, n. 10, p. 1210–1249, http://dx.doi.org/10.2475/10.2010.02
Jahn, B.-M., Chen, P. Y., and Yen, T. P., 1976, Rb-Sr ages of granitic rocks in southeastern China and their tectonic significance: Geological Society of America Bulletin, v. 86, n. 5, p. 763–776, http://dx.doi.org/10.1130/0016-7606(1976)87⟨763:RAOGRI⟩2.0.CO;2
JXBGMR (Jiangxi Bureau of Geology and Mineral Resources), 1984, Regional Geology of Jiangxi Province: Beijing, Geological Publishing House, 921 p. (in Chinese with English abstract).
Li, J., 1993, Tectonic framework and evolution of southeastern China: Journal of Southeast Asian Earth Sciences, v. 8, n. 1–4, p. 219–223, http://dx.doi.org/10.1016/0743-9547(93)90023-I
Li, W.-X., Li, X.-H., and Li, Z.-X., 2005, Neoproterozoic bimodal magmatism in the Cathaysia block of South China and its tectonic significance: Precambrian Research, v. 136, n. 1, p. 51–66, http://dx.doi.org/10.1016/j.precamres.2004.09.008
Li, W. X., Li, X. H., Li, Z. X., and Lou, F. S., 2008, Obduction-type granites within the NE Jiangxi Ophiolite: Implications for the final amalgamation between the Yangtze and Cathaysia blocks: Gondwana Research, v. 13, n. 3, p. 288–301, http://dx.doi.org/10.1016/j.gr.2007.12.010
Li, W. X., Li, X. H., and Li, Z. X., 2010, *Ca.* 850 Ma bimodal volcanic rocks in Northeastern Jiangxi Province, South China: Initial extension during the breakup of Rodinia: American Journal of Science, v. 310, n. 9, p. 951–980, http://dx.doi.org/10.2475/09.2010.08
Li, X. H., 1998, The SHRIMP U–Pb zircon geochronology of Paleoproterozoic plagioclase-amphibolite in the Zhejiang-Fujian area: Journal of Geochemistry, v. 27, n. 4, p. 327–334.
Li, X. H., Zhou, G. Q., and Zhao, J. X., 1994, The zircon U-Pb SHRIMP dating on the Northeastern Jiangxi ophiolite and its tectonic significance: Journal of Geochemistry, v. 23, n. 2, p. 125–131.
Li, X.-H., Li, W.-X., Li, Z.-X., Lo, C.-H., Wang, J., Ye, M.-F., and Yang, Y.-H., 2009, Amalgamation between the Yangtze and Cathaysia blocks in South China: Constraints from SHRIMP U–Pb zircon ages, geochemistry and Nd–Hf isotopes of the Shuangxiwu volcanic rocks: Precambrian Research, v. 174, n. 1–2, p. 117–128, http://dx.doi.org/10.1016/j.precamres.2009.07.004
Li, Z. X., Li, X. H., Kinny, P. D., Wang, J., Zhang, S., and Zhou, H., 2003, Geochronology of Neoproterozoic syn-rift magmatism in the Yangtze Craton, South China and correlations with other continents: evidence for a mantle superplume that broke up Rodinia: Precambrian Research, v. 122, n. 1–4, p. 85–109, http://dx.doi.org/10.1016/S0301-9268(02)00208-5
Li, Z.-X., Li, X.-H., Wartho, J.-A., Clark, C., Li, W.-X., Zhang, C.-L., and Bao, C., 2010, Magmatic and metamorphic events during the early Paleozoic Wuyi-Yunkai Orogeny, southeastern South China: New age constraints and pressure-temperature conditions: Geological Society of America Bulletin, v. 122, n. 5–6, p. 772–793, http://dx.doi.org/10.1130/B30021.1
Liang, D., Meng, Q.-R., Zhang, C.-L., and Liu, X.-M., 2011, Tracing the position of South China block in Gondwna: U-Pb ages and Hf isotopes of Devonian detrital zircons: Gondwana Research, v. 19, n. 1, p. 141–149, http://dx.doi.org/10.1016/j.gr.2010.05.005
Liu, B. J., Xu, X. S., and Pan, X. N., 1993, Deposition of paleo-continents, crustal evolution and metallization: Beijing, Science Press, p. 236 (in Chinese with English abstract).
Ludwig, K. R., 2001, Users Manual for Isoplot/Ex(rev.2.49): A Geochronological Toolkit for Microsoft Excel: Berkeley, California, Berkeley Geochronology Center, Special Publication 1a, p. 55.
Qi, L., and Gregoire, D. C., 2000, Determination of trace elements in twenty six Chinese geochemistry

reference materials by inductively coupled plasma-mass spectrometry: Geostandards Newsletter, v. 24, n. 1, p. 51–63, http://dx.doi.org/10.1111/j.1751-908X.2000.tb00586.X

Qi, L., Jing, H., and Gregoire, D. C., 2000, Determination of trace elements in granites by inductively coupled plasma-mass spectrometry: Talanta, v. 51, n. 3, p. 507–513, http://dx.doi.org/10.1016/S0039-9140(99)00318-5

Ren, J. S., 1964, Preliminary discussion on several problems of Predevonian tectonics of the Southeastern China: Acta Geologica Sinica, v. 44, n. 4, p. 418–430 (in Chinese with English abstract).

Ren, J. S., Chen, T. Y., and Niu, B. G., 1990, The tectonics and mineralization of continental lithosphere in the East China and adjacent region: Beijing, Science Press, 205 p. (in Chinese with English abstract).

Ren, J. S., Niu, B. G., He, Z. J., Xie, G. L., and Liu, Z. G., 1998, Tectonic framework and geodynamic evolution of eastern China, *in* Ren, J. S., and Yang, W. R., editors, The Lithospheric Texture and Tectonic-Magmatic Evolution of the Eastern China: Beijing, Atomic Energy Publishing House, p. 1–12 (in Chinese with English abstract).

Rickwood, P. C., 1989, Boundary lines within petrologic diagrams which use oxides of major and minor elements: Lithos, v. 22, n. 4, p. 247–263, http://dx.doi.org/10.1016/0024-4937(89)90028-5

Rong, J. Y., Chen X., Su, Y. Z., Ni, Y. N., Zhanm R., Chen, T. G., Fu, L. P., Li, R. Y., and Fan, J. X., 2003, Silurian paleogeography of China, *in* Landing, E., and Johnson, M., editors, Silurian Lands and Seas: Paleography outside of Laurentia: New York State Museum Bulletin, v. 493, p. 243–298.

Rong, J. Y., Zhan, R. B., Xu, H. G., Huang, B., and Yu, G. H., 2010, Expansion of the Cathaysia Oldland through the Ordovician-Silurian transition: emerging evidence and possible dynamics: Science in China Series D: Earth Sciences, v. 53, n. 1, p. 1–17, http://dx.doi.org/10.1007/s11430-010-0005-3

Roure, F., Choukroune, P., Berastegui, X., Munoz, J. A., Villien, A., Matheron, P., Bareyt, M., Séguret, M., Camara, P., and Deramond, J., 1989, ECORS Deep seismic data and balanced cross sections: Geometric constraints on the evolution of the Pyrénées: Tectonics, v. 8, n. 1, p. 41–50, http://dx.doi.org/10.1029/TC008i001p00041

Shen, W. Z., Zhu, J. C., and Liu, C. S., 1993, Sm-Nd isotopic study of basement metamorphic rocks in South China and its constraint on material sources of granitoids: Acta Petrologica Sinica, v. 9, n. 2, p. 115–124 (in Chinese with English abstract).

Shen, W. Z., Zhang, F. R., Shu, L. S., and Wang, L. J., 2008, Formation age, geochemical characteristics of the Ninggang granite body in Jiangxi Province and its tectonic significance: Acta Petrologica Sinica, v. 24, n. 10, p. 2244–2254 (in Chinese with English abstract).

Shen, W. Z., Ling, H. F., Shu, L. S., Zhang, F. R., and Xiang, L., 2009. Sm-Nd isotopic compositions of Cambrian-Ordovician strata at the Jinggangshan area in Jiangxi Province: Tectonic implications: Chinese Science Bulletin, v. 54, n. 10, p. 1750–1758, http://dx.doi.org/10.1007/s11434-009-0214-3

Shu, L., and Charvet, J., 1996, Kinematics and geochronology of the Proterozoic Dongxiang-Shexian ductile shear zone: with HP metamorphism and ophiolitic melange (Jiangnan region, South China): Tectonophysics, v. 267, n. 1–4, p. 291–302, http://dx.doi.org/10.1016/S0040-1951(96)00104-7

Shu, L., Faure, M., Jiang, S., Yang, Q., and Wang, Y., 2006, SHRIMP zircon U-Pb age, litho- and biostratigraphic analyses of the Huaiyu Domain in South China—Evidence for a Neoproterozoic orogen, not Late Paleozoic-Early Mesozoic collision: Episodes, v. 29, n. 4, p. 244–252.

Shu, L., Faure, M., Wang, B., Zhou, X., and Song, B., 2008a, Late Paleozoic-Early Mesozoic geological features of South China: Response to the Indosinian collision event in Southeast Asia: Comptes Rendus Geoscience, v. 340, n. 2–3, p. 151–165, http://dx.doi.org/10.1016/j.crte.2007.10.010

Shu, L. S., Zhou, G. Q., Shi, Y. S., and Yin, J., 1994, Study of the high pressure metamorphic blueschist and its Late Proterozoic age in the Eastern Jiangnan belt: Chinese Science Bulletin, v. 39, n. 14, p. 1200–1204.

Shu, L. S., Shi, Y. S., Guo, L. Z., Charvet, J., and Sun, Y., 1995, The Late Proterozoic plate tectonics and collisional kinematics in the middle part of the Jiangnan belt: Nanjing, Nanjing University Publishing House, 174 p. (in Chinese with English abstract).

Shu, L. S., Lu, H. F., Jia, D., Charvet, J., and Faure, M., 1999, Study of the $^{40}Ar/^{39}Ar$ isotopic age for the early Paleozoic tectonothermal event in the Wuyishan region, South China: Journal of Nanjing University (Natural Sciences), v. 35, n. 6, p. 668–674 (in Chinese with English abstract).

Shu, L. S., 2006, Predevonian tectonic evolution of South China: from Cathaysia block to Caledonian period folded orogenic belt: Geological Journal of China Universities, v. 12, n. 4, p. 418–431 (in Chinese with English abstract).

Shu, L. S., Yu, J. H., Jia, D., Wang, B., Shen, W. Z., and Zhang, Y. Q., 2008b, Early Paleozoic orogenic belt in the eastern segment of South China: Geological Bulletin of China, v. 27, n. 10, p. 1581–1593 (in Chinese with English abstract).

Shu, L. S., Deng, P., Yu, J. H., Wang, Y. B., and Jiang, S. Y., 2008c, The age and tectonic environment of the rhyolitic rocks on the western side of Wuyi Mountain, South China: Science in China Series D: Earth Science, v. 51, n. 8, p. 1053–1063, http://dx.doi.org/10.1007/s11430-008-0078-4

Shu, L. S., Zhou, X. M., Deng, P., Wang, B., Jiang, S. Y., Yu, J. H., and Zhao, X. X., 2009, Mesozoic tectonic evolution of the southeast China block: New insights from basin analysis: Journal of Asian Earth Sciences, v. 34, n. 3, p. 376–391, http://dx.doi.org/10.1016/j.jseaes.2008.06.004

Shu, L.-S., Faure, M., Yu, J.-H., and Jahn, B.-M., 2011a, Geochronological and geochemical features of the Cathaysia block (South China): New evidence for the Neoproterozoic breakup of Rodinia: Precambrian Research, v. 187, n. 3–4, p. 263–276, http://dx.doi.org/10.1016/j.precamres.2011.03.003

Shu, L. S., Deng, X. L., Zhu, W. B., Ma, D. S., and Xiao, W. J., 2011b, Precambrian tectonic evolution of the Tarim Block, NW China: new geochronological insights from the Quruqtagh domain: Journal of Asian Earth Sciences, v. 42, n. 5, p. 774–790, http://dx.doi.org/10.1016/j.jseaes.2010.08.018

Sun, X. M., Lu, B. L., Zhang, G. C., Wang, P. J., and Zhang, B., 2013, Structure attribute and evolution of the northern epicontinental basin's basement: Science in China Series D: Earth Sciences.

Taylor, S. R., and McLennan, S. M., 1985, The continental crust: its composition and evolution: Oxford, Blackwell Science, 312 p.
Wang, D., and Shu, L., 2012, Late Mesozoic basin and range tectonics and related magmatism in Southeast China: Geoscience Frontiers, v. 3, n. 2, p. 109–124, http://dx.doi.org/10.1016/j.gsf.2011.11.007
Wang, D. Z., and Zhou, X. M., 2002, Genesis of Late Mesozoic volcanic-intrusive complex of Southeast China and crustal evolution: Beijing, Science Press, 295 p.
Wang, H. Z., and Mo, X. X., 1995, An outline of the tectonic evolution of China: Episodes, v. 18, n. 1–2, p. 6–16.
Wang, J., and Li, Z.-X., 2003, History of Neoproterozoic rift basins in South China: implications for Rodinia break-up: Precambrian Research, v. 122, n. 1–4, p. 141–158, http://dx.doi.org/10.1016/S0301-9268(02)00209-7
Wang, K.-L., O'Reilly, S. Y., Griffin W. L., Chung, S.-L., and Pearson, N. J., 2003, Proterozoic mantle lithosphere beneath the extended margin of the South China Block: *In situ* Re-Os evidence: Geology, v. 31, n. 8, p. 709–712, http://dx.doi.org/10.1130/G19619.1
Wang, X.-L., Zhou, J.-C., Qiu, J.-S., Zhang, W.-L., Liu, X.-M., and Zhang, G.-L., 2006, LA-ICP-MS U–Pb zircon geochronology of the Neoproterozoic igneous rocks from Northern Guangxi Province, South China: Implications for the tectonic evolution: Precambrian Research, v. 145, n. 1–2, p. 111–130, http://dx.doi.org/10.1016/j.precamres.2005.11.014
Wang, X.-L., Zhou, J.-C., Griffin, W. L., Wang, R.-C., Qui, J.-S., O'Rielly, S. Y., Xu, X., Liu, X.-M., and Zhang, G.-L., 2007, Detrital zircon geochronology of Precambrian basement sequences in the Jiangnan orogen: Dating the assembly of the Yangtze and Cathaysia blocks: Precambrian Research, v. 159, n. 1–2, p. 117–131, http://dx.doi.org/10.1016/j.precamres.2007.06.005
Wang, Y., Fan, W., Zhao, G., Ji, S., and Peng, T., 2007, Zircon U-Pb geochronology of gneissic rocks in Yunkai massif and its implications on the Caledonian event in South China: Gondwana Research, v. 12, n. 4, p. 404–416. http://dx.doi.org/10.1016/j.gr.2006.10.003
Wang, Y., Zhang, F., Fan, W., Zhang, G., Chen, S., Cawood, P. A., and Zhang, A., 2010, Tectonic setting of the South China Block in the early Paleozoic: Resolving intracontinental and ocean closure models from detrital zircon U-Pb geochronology: Tectonics, v. 29, n. 6, TC6020, 16 p, http://dx.doi.org/10.1029/2010TC002750
Wang, Y., Fan, W., Zhang, G., and Zhang, Y., 2013, Phanerozoic tectonics of the South China Block: Key observations and controversies: Gondwana Research, v. 23, n. 4, p. 1273–1305 http://dx.doi.org/10.1016/j.gr.2012.02.019
Wu, H., 2005, Discussion on tectonopalaeogeography of Lower Yangtze area during the Caledonian Period: Journal of Palaeogeography, v. 7, n. 2, p. 243–248, http://dx.doi.org/10.7605/gdlxb.2005.02.009
Xiang, L., and Shu, L. S., 2010, Pre-Devonian tectonic evolution of the eastern South China Block: Geochronological evidence from detrital zircons: Science China: Earth Sciences, v. 53, n. 10, p. 1427–1444, http://dx.doi.org/10.1007/s11430-010-4061-5
Xiao, W., and He, H., 2005, Early Mesozoic thrust tectonics of the northwest Zhejiang region (Southeast China): Geological Society of America Bulletin, v. 117, n. 7–8, p. 945–961, http://dx.doi.org/10.1130/B25417.1
Xu, B., Guo, L. Z., and Shi, Y. S., 1992, Proterozoic terranes and multiphase collision orogens in Anhui-Zhejiang-Jiangxi area: Beijing, Geological Publishing House, 112 p.
Xu, K. Q., Liu, Y. J., and Yu, S. J., 1960, Discussion on the Caledonian Period Granite in South Jiangxi: Geological Review, v. 20, n. 3, p. 112–114 (in Chinese).
Xu, K. Q., Sun, N., Wang, D. Z., and Hu, S. X., 1963, Discussion on the intruded ages, lithological features, distribution rules and metallogic speciality of multiple cycle granitoids in South China: Acta Geologica Sinica, v. 43, n. 1–2, p. 141–155.
Xu, X., O'Reilly, S. Y., Griffin, W. L., Deng, P., and Pearson, N. J., 2005, Relict Proterozoic basement in the Nanling Mountains (SE China) and its tectonothermal overprinting: Tectonics, v. 24, n. 2, TC2003, 16 p., http://dx.doi.org/10.1029/2004TC001652
Xu, X., Due, D., Li, Y., Hu, P., and Chen, N., 2013, Neoproterozoic sequences along the Dexing-Huangshan fault zone in the eastern Jiangnan orogen, South China: Geochronological and geochemical constraints: Gondwana Research, http://dx.doi.org/10.1016/j.gr.2013.03.020
Xu, X. B., Zhang, Y. Q., Shu, L. S., and Jia, D., 2011, La-ICP-MS U-Pb and $^{40}Ar/^{39}Ar$ geochronology of the sheared metamorphic rocks in the Wuyishan: Constraints on the timing of early Paleozoic and early Mesozoic tectono-thermal events in SE China: Tectonophysics, v. 501, n. 1–4, 71–86, http://dx.doi.org/10.1016/j.tecto.2011.01.014
Yao, J., Shu, L., and Santosh, M., 2011, Detrital zircon U-Pb geochronology, Hf-isotopes and geochemistry—New clues for the Precambrian crustal evolution of Cathaysia block, South China: Gondwana Research, v. 20, n. 2–3, p. 553–567, http://dx.doi.org/10.1016/j.gr.2011.01.005
Yao, J. L., Shu, L. S., Santosh, M., and Li, J. Y., 2012, Precambrian crustal evolution of the South China Block and its relation to supercontinent history: Constraints from U-Pb ages, Lu-Hf isotopes and REE geochemistry of zircons from sandstones and granodiorite: Precambrian Research, v. 208–211, p. 19–48, http://dx.doi.org/10.1016/j.precamres.2012.03.009
Yin, H. F., Wu, S. B., Du, Y. S., and Peng, Y. Q., 1999, South China defined as part of Tethyan archipelagic ocean system: Earth Science-Journal of China University of Geosciences, v. 24, n. 1, p. 1–12.
YNBGMR (Yunnan Bureau of Geology and Mineral Resources), 1988, Regional geology of Yunnan Province: Beijing, Geological Publishing House, 727 p. (in Chinese with English abstract).
Yu, J. H., O'Reilly, Y. S., Wang, L. J., Griffin, W. L., Jiang, S. Y., Wang, R. C., and Xu, X. S., 2007, Finding of ancient materials in Cathaysia and implication for the formation of Precambrian crust: Chinese Science Bulletin, v. 52, n. 1, p. 13–22, http://dx.doi.org/10.1007/s11434-007-0008-4
Yu, J.-H., Wang, L., O'Reilly, S. Y., Griffin, W. L., Zhang, M., Li, C., and Shu, L., 2009, A Paleoproterozoic

orogeny recorded in a long-lived cratonic remnant (Wuyishan terrane), eastern Cathaysia block, China: Precambrian Research, v. 174, n. 3–4, p. 347–363, http://dx.doi.org/10.1016/j.precamres.2009.08.009

Yuan, H.-L., Gao, S., Dai, M.-N., Zong, C.-L., Günther, D., Fontaine, G. H., Liu, X.-M., and Diwu, C. R., 2008, Simultaneous determinations of U–Pb age, Hf isotopes and trace element compositions of zircon by excimer laser ablation quadrupole and multiple collector ICP–MS: Chemical Geology, v. 247, n. 1–2, p. 100–118, http://dx.doi.org/10.1016/j.chemgeo.2007.10.003

Zhang, F. R., Shu, L. S., Wang, D. Z., and Shen, W. Z., 2009, Discussions on the tectonic setting of Caledonian granitoids in the eastern segment of South China: Earth Science Frontiers, v. 16, n. 1, p. 247–259 (in Chinese with English abstract).

Zhang, F. R., Shu, L. S., Wang, D. Z., Shen, W. Z., Yu, J. H., and Xie, L., 2010a, Study on geochronological, geochemical features and genesis of the Fufang granitic pluton in the Jiangxi Province, South China: Geological Journal of China Universities, v. 16, n. 2, p. 161–176 (in Chinese with English abstract).

Zhang, F. R., Shen, W. Z., Shu, L. S., and Xiang, L., 2010b, Geochemical features of early Paleozoic granites in Jiangxi Province and their geological significances: Acta Petrologica Sinica, v. 26, n. 12, p. 3456–3468 (in Chinese with English abstract).

Zhang, G. W., Guo, A. L., Wang, Y. J., Li, S. Z., Dong, Y. P., Liu, S. F., He, D. F., Cheng, S. Y., Lu, R. K., and Yao, A. P., 2013, Tectonics of South China Continent and its Implications: Science in China-Earth Sciences, v. 56, n. 11, p. 1804–1828, http://dx.doi.org/10.1007/s11430-013-4679-1

Zhang, S.-B., and Zheng, Y.-F., 2013, Formation and evolution of Precambrian continental lithosphere in South China: Gondwana Research, v. 23, n. 4, p. 1241–1260, http://dx.doi.org/10.1016/j.gr.2012.09.005

Zhang, S. G., and Yan, H. J., 2005, A brief introduction to international stratigraphic chart and global stratotype section and points: Journal of Stratigraphy, v. 29, p. 188–203 (in Chinese with English abstract).

Zhang, Y., Shu, L. S., and Chen, X. Y., 2011, Study of geochemistry, geochronology and petro-genesis of the early Paleozoic granitic plutons in the central-southern Jiangxi Province: Science China: Earth Sciences, v. 54, n. 10, 1492–1510, http://dx.doi.org/10.1007/s11430-011-4249-3

Zhou, X. M., Sun, T., Shen, W. Z., Shu, L. S., and Niu, Y. L., 2006. Petrogenesis of Mesozoic granitoids and volcanic rocks in South China: A response to tectonic evolution: Episodes, v. 29, p. 26–33.

ZJBGMR (Zhejiang Bureau of Geology and Mineral Resources), 1989, Regional geology of Zhejiang Province: Beijing, Geological Publishing House, 688 p. (in Chinese with English abstract).